LHC data interpretation within the 2HDM type II via a new analysis toolkit

E. Accomando,[1,*] C. Byers,[1,†] D. Englert,[1,2,‡] J. Hays,[2,§] and S. Moretti[1,3,4,¶]

[1] *School of Physics & Astronomy, University of Southampton, Highfield, Southampton SO17 1BJ, UK*
[2] *Particle Physics Research Centre, School of Physics and Astronomy, Queen Mary University of London, Mile End Road, London E1 4NS, UK*
[3] *Particle Physics Department, Rutherford Appleton Laboratory, Chilton, Didcot, Oxon OX11 0QX, UK*
[4] *Department of Physics and Astronomy, Uppsala University, Box 516, SE-751 20 Uppsala, Sweden*

We review the status of the 2-Higgs Doublet Model (2HDM) Type-II, in the light of the current experimental results and various theoretical consistency conditions. Compared to the existing literature, in this paper we apply for the first time a new method that can improve the standard procedure for setting bounds on the 2HDM parameter space, as no experimental evidence has been found so far. Our new numerical framework, called `Magellan`, and statistical techniques can be applied to any Beyond the Standard Model (BSM) scenario. Here, we take as testing ground the 2HDM, particularly as it is physically interesting and moreover characterised by a far from trivial multi-dimensional parameter space where the effectiveness of the new methods can be proved. `Magellan` uses a Markov Chain Monte Carlo technique for scanning the parameter space and leverages the use of data processing and visualisation methods, allowing the user to perform inference on the model in a complete and efficient way. The novelty of the proposed method is that the parameter space of any BSM theory can be projected onto any bi-dimensional plane while still retaining all underlying attributes of those points, so that it is possible to investigate the associations between the properties of the various lower dimensional sub-spaces of the complete parameter space. The `Magellan`'s website interactive dashboards can be accessed via a public link. Through this website, the user can explore the full parameter space and exploit the phenomenological features of a BSM model with ease.

I. INTRODUCTION

The discovery of a Higgs boson at the Large Hadron Collider (LHC) has been a triumph for particle physics [1, 2], revealing that the masses of the fundamental particles in Nature are indeed generated through the Higgs mechanism of (spontaneous) Electro-Weak Symmetry Breaking (EWSB). This particle eventually revealed itself to have properties close to those of the Standard Model (SM) Higgs state. However, even if technically possible, it is rather unnatural thinking that the discovered state would ultimately complete the particle physics scenario. Such a light Higgs state leaves in fact the hierarchy problem unresolved, that is, the great disparity between the Higgs mass itself (125 GeV) and the Planck scale (of order 10^{19} GeV). Under the assumption that the discovered Higgs state is of a fundamental nature, i.e., not a composite state, in order to surpass the hierarchy problem, one has to invoke Beyond the SM (BSM) scenarios that inevitably involve an enlarged Higgs sector. One could have any number of singlet Higgs fields and/or Higgs doublets.

In this paper, we consider the presence of a second Higgs doublet, thereby introducing a generic 2-Higgs Doublet Model (2HDM). The presence of a second Higgs doublet naturally arises in many models of BSM physics that can remedy several of the flaws of the SM. Just to cite a few of these, a class of axion models [3, 4], which can explain the lack of observed CP violation in the strong sector, and certain realisations of composite Higgs models with pseudo-Nambu-Goldstone bosons [5–9], can both give rise to an effective low-energy theory with two Higgs doublets. The additional source of CP violation present in this type of enlarged (pseudo)scalar sector could further provide an explanation of the matter-antimatter asymmetry. Particular realisations of the 2HDM also have the appealing features of being able to explain neutrino mass generation [10], to provide a candidate for dark matter [11] or to accommodate the muon $g-2$ anomaly [12–14]. While all these phenomena cannot all be addressed simultaneously by the 2HDM, it is worth mentioning that the Higgs sector embedded in it can be found in realisations of complete

[*] E-mail: e.accomando@soton.ac.uk
[†] E-mail: c.byers@soton.ac.uk
[‡] E-mail: david.englert@soton.ac.uk, d.englert@qmul.ac.uk
[§] E-mail: j.hays@qmul.ac.uk
[¶] E-mail: s.moretti@soton.ac.uk, stefano.moretti@stfc.ac.uk, stefano.moretti@physics.uu.se

theories, like Supersymmetry, e.g., it is well known that the Minimal Supersymmetric Standard Model (MSSM) requires the existence of two doublets to generate the mass of both up-type and down-type quarks and charged leptons. In this case, the Yukawa couplings should have Type-II values. The representative model chosen in this paper, the 2HDM Type-II, would therefore coincide with the MSSM [15, 16] in the sparticle decoupling limit where the Supersymmetry scale is assumed to be much higher than the EW one. This coincidence does not spoil the pure generality of the chosen 2HDM representation of the scalar sector, embedded in the wide variety of models concisely recalled above.

From the experimental point of view, the additional four Higgs states of a generic 2HDM [15, 17] provide a range of observables through which all the above theoretical models could in principle be tested, or at least have a first evidence of their validity through their scalar sector. Hence, it is worthwhile investigating in detail the scope of the LHC in discovering the new Higgs bosons described by the 2HDM generic representation.

There exists a vast literature on the phenomenological analyses setting bounds on the 2HDM parameter space, as no experimental evidence has been found so far. The last two decades have seen the implementation and development of global fits, which collect the data coming from different experiments and make rigorous statistical analyses to extract limits on BSM theories. The package GFitter [18] was a pioneer in releasing a global EW fit to constrain New Physics predicted by a variety of models, including the 2HDM. Other toolkits are published in the literature, with their main focus centred on Supersymmetry and its numerous variants. A global analysis of Supersymmetry is provided by SFitter [19], SuperBayeS [20–22], Fittino [23–25], Lilith [26, 27] and MasterCode [28–32]. A much wider range of BSM theories is covered by the package Gambit [33, 34], a global fitting software framework characterised by theory flexibility and straightforward extension to new observables and external interfaces. Bounds on the MSSM are addressed by Gambit in Ref. [34] and limits on the 2HDM are derived in Ref. [35], specifically.

The standard procedure, generally adopted by global fitting packages, makes use of all relevant experimental data and theoretical arguments that can constrain the model. These constraints can be categorised into the following three main sources: measurements of the discovered 125 GeV Higgs boson properties (i.e., production and decay signal strengths), direct and indirect searches for the extra Higgs bosons present in the model and, finally, theory considerations based on perturbativity, unitarity, triviality and vacuum stability. The statistical analysis is then performed, with the likelihood function expressing the plausibilities of different parameter values for the given sample(s) of data. As the 2HDM parameter space is six-dimensional, the standard way of extracting bounds is projecting the full parameter space onto bi-dimensional planes, defined by any two model parameters. In doing so, the statistical procedure is maximising the (log-)likelihood on all the other four remaining parameters.

In this paper, we apply for the first time a new method that can improve this standard procedure. Our new tools and statistical techniques can be applied to any BSM scenarios. Here, we take as testing ground the 2HDM, particularly as it is physically interesting and moreover characterised by a multi-dimensional parameter space. This latter feature allows us to prove the effectiveness and efficiency of our new approach in a far from trivial setup. First of all, we perform an efficient scanning of the parameter space through a Markov Chain Monte Carlo (MCMC) approach with `T3PS` [36]. After this first step, instead of projecting the parameter space onto bi-dimensional planes by maximising the (log-)likelihood over the other remaining parameters, we keep the full punctual information on all the model parameters, simultaneously. We introduce effective data processing and visualisation methods based on `pandas` [37], `matplotlib` [38], `bokeh` [39] and `holoviews` [40]. With the help of these packages and the wrapper framework called `Magellan`, the parameter space of any BSM theory can be projected onto any bi-dimensional plane while still retaining all underlying attributes of those points, so that it is possible to investigate the associations between the properties of the various lower dimensional sub-spaces of it. This constitutes the novelty of our method. The code `Magellan` is not published yet [41]. However, its website interactive dashboards can be accessed via the link given in Ref. [42]. We have moreover created an open-access repository in Zenodo. There, we have published the datasets generated by `Magellan`. The MCMC scan of the 2HDM Type-II parameter space is stored in a HDF5 file and instructions are given to load the dataset as a pandas data-frame. Through the `Magellan` website, the user can explore the complete parameter space at once and exploit the phenomenological features of the model with ease.

To envisage the wider use of the proposed toolkit, we highlight that applications of `Magellan` to BSM theories other than the 2HDM presented in this paper are already well documented. The first one addresses the analysis of the Higgs boson pair production in six different channels. In this case, the toolkit has been used to extract the excluded regions in the parameter space of the EWK-singlet model and the hMSSM model. This analysis has been published by ATLAS [43]. The second application concerns the analysis of the extra CP-even Higgs decaying into two light Higgses at the LHC within the 2HDM Type-II. This analysis is already public on the Magellan website. There, also the analyses of both the heavy CP-even and CP-odd Higgs decaying into tau pairs are published. These latter studies represent extensions of the main analysis carried out in this paper which, for illustrative purposes, is focussed on the associated production $pp \to Zh \to 4f$ within the Type-II 2HDM [44].

The plan of the paper is as follows. In Section 2, we describe the 2HDM Type-II, as explained, taken as prototypical example to illustrate the described approach. In Section 3, the scanning procedure is specified. Section 4 enumerates

the theoretical and experimental constraints that are taken into account during the paremeter space scans. Section 5 shows how data interpretation is facilitated by the new toolkit. Finally, in Section 6, we conclude.

II. THE 2HDM

In this section we give a brief introduction to the 2HDM, with a focus on the aspects relevant to our analysis. Extensive reviews of the 2HDM can be found in Refs. [15–17]. An important feature of the model is the number of degrees of freedom (d.o.f.) of the fields, which we can be enumerated before and after the spontaneous breaking of the EW symmetry due to the shape of the Higgs potential. Initially, we have two complex doublets, Φ_1 and Φ_2, giving eight d.o.f. in total. After EWSB, the spectrum contains two CP-even scalars h and H, one pseudoscalar A and two charged Higgs bosons $H^\pm$ (i.e., five d.o.f.). The Goldstone bosons of the theory will then become the longitudinal components of the weak $W^\pm$ and Z bosons (three d.o.f). Hence, the total number of d.o.f. is unchanged.

The most general renormalisable (i.e., quartic) scalar potential of two doublets can be written as

$$\begin{aligned}\mathcal{V}_{gen} = & m_{11}^2\Phi_1^\dagger\Phi_1 + m_{22}^2\Phi_2^\dagger\Phi_2 - \left[m_{12}^2\Phi_1^\dagger\Phi_2 + \text{h.c}\right] + \\ & + \frac{1}{2}\lambda_1\left(\Phi_1^\dagger\Phi_1\right)^2 + \frac{1}{2}\lambda_2\left(\Phi_2^\dagger\Phi_2\right)^2 + \lambda_3\left(\Phi_1^\dagger\Phi_1\right)\left(\Phi_2^\dagger\Phi_2\right) + \lambda_4\left(\Phi_1^\dagger\Phi_2\right)\left(\Phi_2^\dagger\Phi_1\right) + \\ & + \left\{\frac{1}{2}\lambda_5\left(\Phi_1^\dagger\Phi_2\right)^2 + \left[\lambda_6\left(\Phi_1^\dagger\Phi_1\right) + \lambda_7\left(\Phi_2^\dagger\Phi_2\right)\right]\Phi_1^\dagger\Phi_2\right\},\end{aligned} \tag{1}$$

where m_{11}^2, m_{22}^2, m_{12}^2 are mass squared terms and λ_i ($i = 1, ..., 7$) are dimensionless quantities describing the coupling of the order-4 interactions. Of all such parameters, 6 are real (m_{11}^2, m_{22}^2, λ_i with $i = 1, ..., 4$) and 4 are a priori complex (m_{12}^2 and λ_i with $i = 5, ..., 7$). Therefore, in general, the model has 14 free parameters. Under appropriate manipulations, this number can however be reduced.

Following Ref. [45], to start with, one can diagonalise the quadratic part of the potential in the (Φ_1, Φ_2) space, removing the m_{12}^2 term, thus getting rid of 2 parameters. Then, one can make a relative $U(1)$ transformation on Φ_1 or Φ_2, making λ_5 real, hence down to 11 parameters. Next, by removing CP violation, the number of free parameters reduces to 9, as this requires making one neutral Higgs state decouple from both VV ($VV = W^+W^-$ and ZZ) and H^+H^- interactions. Furthermore, the Yukawa matrices corresponding to the two doublets are not simultaneously diagonalisable, which can pose a problem, as the off-diagonal elements lead to tree-level Higgs mediated Flavour Changing Neutral Currents (FCNCs) on which severe experimental bounds exist. The Glashow-Weinberg-Paschos (GWP) theorem [46, 47] states that this type of FCNCs is absent if at most one Higgs multiplet is responsible for providing mass to fermions of a given electric charge. This GWP condition can be enforced by a discrete $\mathbb{Z}_2$-symmetry ($\Phi_1 \to +\Phi_1$ and $\Phi_2 \to -\Phi_2$) on the doublets, in which case the absence of FCNCs is natural. The soft $\mathbb{Z}_2$-symmetry breaking condition relies on the existence of a basis where $\lambda_6 = \lambda_7 = 0$. Therefore, one loses 2 additional parameters potentially reducing further their overall number down to 7, yet, allowing for a softly broken $\mathbb{Z}_2$-symmetry, as customarily done to enable EWSB compliant with experimental measurements, leads to 8 parameters.

However, after EWSB, each scalar doublet acquires a Vacuum Expectation Value (VEV) that can be parametrised as follows:

$$\langle\Phi_1\rangle = \frac{v}{\sqrt{2}}\begin{pmatrix}0\\ \cos\beta\end{pmatrix} \qquad \langle\Phi_2\rangle = \frac{v}{\sqrt{2}}\begin{pmatrix}0\\ \sin\beta\end{pmatrix}, \tag{2}$$

where the angle β determines the ratio of the two doublet VEVs, v_1 and v_2, through the definition of $\tan\beta = v_2/v_1$, and where $v = 246$ GeV is a fixed value, thereby giving a final count of 7 free parameters.

Under the above conditions, there are several alternative bases in which the 2HDM can be described: the *general parametrisation* (as given above in terms of m_{ij}^2 and λ_is), the *Higgs basis*, where one of the doublets gets zero VEV, and the *physical basis*, where one uses the physical masses of the scalars. However, in the light of the discovery of the 125 GeV Higgs boson, herein the h state, it is customary to parametrise the theory using the *hybrid basis* [48], where the parameters provide a convenient choice to give a direct control on both the CP-even and CP-odd Higgs masses, the hVV couplings ($V = W^\pm, Z$), the $Aq\bar{q}$ vertices and the Higgs quartic couplings. The parameters in this basis are:

$$\underbrace{m_h,\quad m_H}_{\text{CP-even Higgs masses}} \quad , \quad \underbrace{\cos(\beta-\alpha)}_{\substack{\text{determines the}\\ g_{hVV}\ \&\ g_{HVV}\ \text{couplings}}} \quad , \quad \underbrace{\tan\beta}_{\text{ratio of the vevs}} \quad , \quad \underbrace{Z_4,\quad Z_5,\quad Z_7,}_{\substack{\text{Higgs self-coupling}\\ \text{parameters}}} \tag{3}$$

Model	h			H			A		
	u	d	l	u	d	l	u	d	l
Type-I	$\frac{\cos\alpha}{\sin\beta}$	$\frac{\cos\alpha}{\sin\beta}$	$\frac{\cos\alpha}{\sin\beta}$	$\frac{\sin\alpha}{\sin\beta}$	$\frac{\sin\alpha}{\sin\beta}$	$\frac{\sin\alpha}{\sin\beta}$	$\cot\beta$	$-\cot\beta$	$-\cot\beta$
Type-II	$\frac{\cos\alpha}{\sin\beta}$	$-\frac{\sin\alpha}{\cos\beta}$	$-\frac{\sin\alpha}{\sin\beta}$	$\frac{\sin\alpha}{\sin\beta}$	$\frac{\cos\alpha}{\sin\beta}$	$\frac{\cos\alpha}{\sin\beta}$	$\cot\beta$	$\tan\beta$	$\tan\beta$
Type-III	$\frac{\cos\alpha}{\sin\beta}$	$\frac{\cos\alpha}{\sin\beta}$	$-\frac{\sin\alpha}{\sin\beta}$	$\frac{\sin\alpha}{\sin\beta}$	$\frac{\sin\alpha}{\sin\beta}$	$\frac{\cos\alpha}{\cos\beta}$	$-\cot\beta$	$\cot\beta$	$-\tan\beta$
Type-IV	$\frac{\cos\alpha}{\sin\beta}$	$-\frac{\sin\alpha}{\cos\beta}$	$\frac{\cos\alpha}{\sin\beta}$	$\frac{\sin\alpha}{\sin\beta}$	$\frac{\cos\alpha}{\cos\beta}$	$\frac{\sin\alpha}{\sin\beta}$	$-\cot\beta$	$-\tan\beta$	$\cot\beta$

Table I: Couplings of the neutral Higgs bosons to fermions, normalised to the corresponding SM value (m_f/v) in the 2HDM Type-I, II, III and IV.

with $m_H \geq m_h$, $0 \leq \beta \leq \pi/2$ and $0 \leq \sin(\beta-\alpha) \leq 1$. The remaining (pseudo)scalar masses can be expressed in terms of the quartic scalar couplings in the Higgs basis:

$$m_A^2 = m_H^2 \sin^2(\beta-\alpha) + m_h^2 \cos^2(\beta-\alpha) - Z_5 v_1^2, \tag{4}$$

$$m_{H^\pm}^2 = m_A^2 - \frac{1}{2}(Z_4 - Z_5)v^2. \tag{5}$$

In the hybrid basis, by swapping the self-couplings Z_4 and Z_5 with the scalar masses given above, the 7 free parameters can be recast into 4 physical masses and 3 parameters that are related to the couplings of the scalars to gauge bosons, fermions and scalars themselves, respectively:

$$m_h,\ m_H,\ m_A,\ m_{H^\pm},\ \cos(\beta-\alpha),\ \tan\beta,\ Z_7. \tag{6}$$

In the above list, Z_7 enters only the triple and quartic scalar interactions. Finally, as m_h has been measured with excellent accuracy at the LHC, the number of parameters defining the scalar potential comes down to 6.

Beside the (pseudo)scalar fields, also fermions are required to have a definite charge under the discrete $\mathbb{Z}_2$-symmetry. The different assignments of the $\mathbb{Z}_2$-charge in the fermion sector give rise to the four different types of 2HDM. The couplings of the neutral Higgses to fermions, normalised to the corresponding SM value (m_f/v, henceforth, denoted by κ_{hqq} for the case of the SM-like Higgs state coupling to a quark q, where $q = d, u$), can be found in Tab. I.

As intimated, in the remainder of this paper, we will concentrate on the 2HDM Type-II. There are two limiting scenarios, giving rise to two distinct regions in the $(\cos(\beta-\alpha), \tan\beta)$ parameter plane [49]. They can be understood by examining the behaviour of κ_{hqq} as a function of the angles α and β. Taking the limits $\beta-\alpha \to \frac{\pi}{2}$ (upper lines in the upcoming figure) and $\beta+\alpha \to \frac{\pi}{2}$ (lower lines in the upcoming figure), the couplings become (recall Tab. I):

$$\begin{aligned}
\kappa_{hdd} = -\frac{\sin\alpha}{\cos\beta} &= \sin(\beta-\alpha) - \cos(\beta-\alpha)\tan\beta \xrightarrow[\beta-\alpha=\frac{\pi}{2}]{} 1 \text{ (middle-region)},\\
&= -\sin(\beta+\alpha) + \cos(\beta+\alpha)\tan\beta \xrightarrow[\beta+\alpha=\frac{\pi}{2}]{} -1 \text{ (right-arm)},\\
\kappa_{huu} = \frac{\cos\alpha}{\sin\beta} &= \sin(\beta-\alpha) + \cos(\beta-\alpha)\cot\beta \xrightarrow[\beta-\alpha=\frac{\pi}{2}]{} 1 \text{ (middle-region)},\\
&= \sin(\beta+\alpha) + \cos(\beta+\alpha)\cot\beta \xrightarrow[\beta+\alpha=\frac{\pi}{2}]{} 1 \text{ (right-arm)}.
\end{aligned} \tag{7}$$

The dependence of κ_{hdd} and κ_{huu} on $\cos(\beta-\alpha)$ and $\tan\beta$ is illustrated in Fig. 1. The $\beta-\alpha \to \frac{\pi}{2}$ case corresponds to the "middle-region", which is the SM limit of the theory. In the right-hand side plot of Fig. 1, this domain is identified by the contour region where $0.9 \leq \kappa_{hdd} \leq 1.1$, that is, assuming a range within 10% of the SM couplings. The $\beta+\alpha \to \frac{\pi}{2}$ case corresponds to the "right-arm", where one gets an opposite sign for the coupling between the SM-like Higgs h and the down-type quarks, relative to the SM value. This is called the wrong-sign Yukawa coupling scenario. In the right-hand side plot of Fig. 1, this region is represented by the narrow arm (or tongue) where the coupling is negative and assuming again a range within 10% of the SM coupling values: $-1.1 \leq \kappa_{hdd} \leq -0.9$. Both the alignment and the wrong-sign regions are well within the O(10%) discrepancy from the corresponding SM value allowed for the coupling of the SM-like Higgs to the up-type quarks, κ_{huu}, as shown in the left-hand plot of Fig. 1.

The most up-to-date 125 GeV Higgs combined signal strength analyses from ATLAS [50] and CMS [51], interpreted in the 2HDM Type-II can be seen in Fig. 2, where it is found that the hypotheses of $\kappa_{hdd} = 1$ and $\kappa_{hdd} = -1$ are still both allowed. On the theory side, an interesting study [52] based on Renormalisation Group Equations (RGEs)

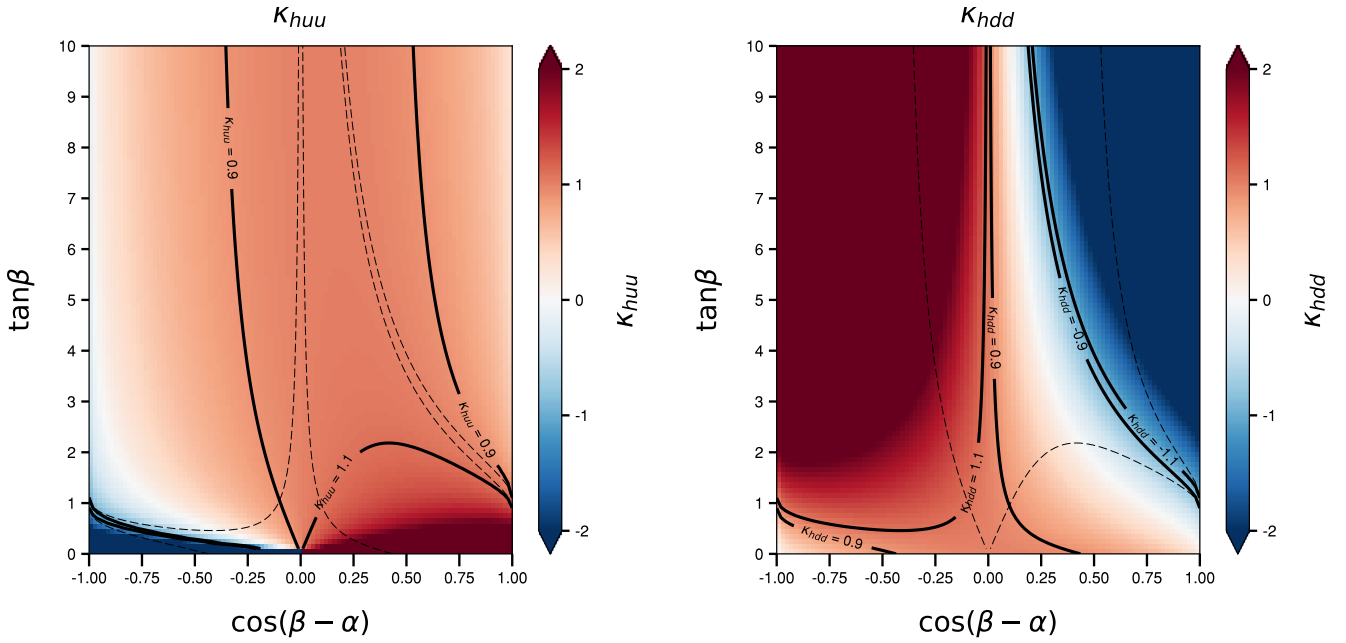

Figure 1: Light CP-even Higgs couplings to the up-type (left) and down-type (right) quarks, normalised to the corresponding SM value, in the $(\cos(\beta-\alpha), \tan\beta)$ plane.

has shown that, if one requires the model to be valid up to higher energies (beyond 1 TeV), the allowed parameter space shrinks to the positive sign of $\kappa_{huu}/\kappa_{hdd}$, otherwise called the alignment region. Below the TeV energy scale, both the alignment and wrong-sign scenario are valid. From a more phenomenological point of view, many analyses have been performed to constrain these two domains. In particular, the importance of the decay channels of the two extra neutral Higgses, A and H, in the wrong-sign limit of the model has been clearly illustrated in Ref. [53]. Here, we intend to revisit in detail how the constraints onto the 2HDM Type-II parameter space are normally drawn and how they can be improved upon using our new framework, i.e., `Magellan`. In the next section, we describe the methodology and the tools employed to perform our scans.

III. MAGELLAN: GLOBAL SCAN FOR BOUNDS EXTRACTION AND DATA INTERPRETATION

In this section, we describe a new methodology that can be employed to explore the parameter space of any BSM theory. Our novel framework, `Magellan`, is indeed designed for a twofold scope. Firstly, it allows one to easily import any new experimental results so as to interpret these within any given model and derive bounds on the corresponding parameter space. Secondly, `Magellan` can quickly predict the regions of the latter that can be accessible in a given search with the actual luminosity at hand and show therein the characteristics of the new particles to be searched for (e.g., mass, width, decay rates, etc.) thus allowing to improve the data analysis.

In order to illustrate the model exploration approach adopted by `Magellan` [42], we take as an example the 2HDM Type-II. Within this new interactive framework, the latest limits on this model are then derived to show the effectiveness of the new method. The key starting point is implementing all existing constraints, from theory and experiment. In order to scan over the 2HDM parameter space, we use a MCMC based on `T3PS` [36] for parallel processing of parameter scans. This tool makes use of the standard Metropolis-Hastings [54, 55] algorithm that is briefly summarised below.

- **Step 0)** Draw a point from the prior distribution $\pi(\theta)$, which will serve as the starting point of the chain. The likelihood corresponding to this point is $\mathcal{L}(\theta|d)$.
- **Step 1)** Propose a new candidate point θ', taken from the proposal distribution $q(\theta', \theta)$. In our case $q(\theta', \theta)$ is a Gaussian distribution, centered around the previous point θ with a standard deviation of a, commonly referred to as the *step-size*. The likelihood corresponding to the new point is $\mathcal{L}(\theta'|d)$.

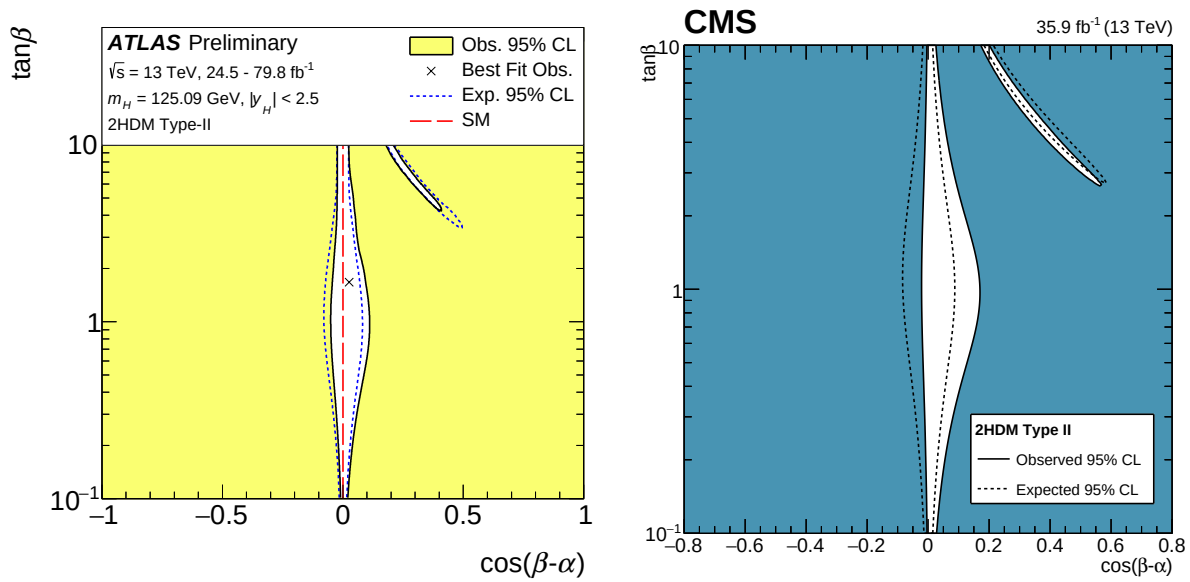

Figure 2: Allowed regions of $(\cos(\beta-\alpha), \tan\beta)$ parameters in 2HDM Type-II, obtained from the compatibility with the observed couplings of the 125 GeV boson, when identified as the light Higgs boson, h of the model. The plot show the most up-to-date available results from ATLAS [50] and CMS [51], seen on the left and right plot respectively.

- **Step 2)** Calculate the ratio of the posterior probabilities corresponding to the two points: $r = \frac{\mathcal{L}(d|\theta')\pi(\theta')q(\theta',\theta)}{\mathcal{L}(d|\theta)\pi(\theta)q(\theta',\theta)}$. In the Metropolis-Hastings algorithm, $q(\theta',\theta)$ is symmetric, therefore it drops out in the ratio.
- **Step 3)** If $r \geq 1$, then accept the new proposal, otherwise accept the candidate with a probability of r. If the point is rejected repeat the process from **Step 1)**.
- **Step 4)** Once a new candidate is found, add it to the chain and repeat the process from **Step 1)**.

The likelihood function, $\mathcal{L}(d|\theta)$, is constructed using the experimental χ^2 values coming from the Higgs coupling measurements and the fit to the S, T and U parameters of the EW Precision Observables (EWPOs). The likelihood is defined as:

$$\mathcal{L} = \exp\left(-\frac{\chi^2_{\rm tot}}{2}\right), \tag{8}$$

where $\chi^2_{\rm tot} = \chi^2_{HS} + \chi^2_{ST}$, with χ^2_{HS} being the χ^2 value extracted from measurements of the h couplings entering the production and decays modes of the SM-like Higgs state discovered at CERN. We have used `HiggsSignals` 2 [56] beta version, which includes experimental data tables collected until September 2018. `HiggsSignals` compares the 2HDM predictions for the scalar sector with the SM-like Higgs signal rate and mass measurements at the LHC, giving rise to a likelihood estimate. Recently, they have released a validation (see Ref. [57]) against the ATLAS and CMS combined analysis of the LHC Run1 data at 7 and 8 TeV [58, 59]. An update for the Run2 data was still unpublished at the time of writing. We have however checked the consistency of our results, obtained then via a link to `HiggsSignals`, against the experimental fits at Run2. The S and T parameter compatibility measure (U is irrelevant for our purposes) χ^2_{ST} is:

$$\chi^2_{ST} = \frac{(S - S^{\rm exp}_{\rm best\ fit})^2}{\sigma^2_S(1-\rho^2_{ST})} + \frac{(T - T^{\rm exp}_{\rm best\ fit})^2}{\sigma^2_T(1-\rho^2_{ST})} - 2\rho_{ST}\frac{(S - S^{\rm exp}_{\rm best\ fit})(T - T^{\rm exp}_{\rm best\ fit})}{\sigma_T\sigma_S(1-\rho^2_{ST})}, \tag{9}$$

where the best fit values $S^{\rm exp}_{\rm best\ fit}$ and $T^{\rm exp}_{\rm best\ fit}$, their uncertainties $\sigma_{S/T}$ and the correlation parameter, ρ^2_{ST}, are taken from the fit result of the Gfitter group [60].

Parameter	min	max	step-size
Z_7	-10.0	10.0	0.2
m_H [GeV]	150	1000.0	20.0
$m_{H^\pm}$ [GeV]	500	1000.0	20.0
m_A [GeV]	100	1000.0	20.0
$\cos(\beta-\alpha)$	-1.0	1.0	0.03
$\tan\beta$	0.5	30.0	0.5

Table II: Range and step-size of the 6-dimensional 2HDM parameters used in the MCMC scan.

α	α_s	$\alpha_{\rm EM} \equiv \alpha(Q^2=0)$	m_t [GeV]	m_h [GeV]
1/127.934	0.119	1/137.035997	172.5	125.09

Table III: Physical parameters kept fixed in our scans.

One naturally concentrates on the experimental observables where the discovered h state enters. However, searches for additional Higgs states, both neutral and charged (at present yielding null results in either case), once interpreted in a specific theoretical model, can force constraints onto its parameter space. Hence, these ought to be included as well. We have done so here using the program `HiggsBounds` 4 [61], which tests the model against the exclusion limits extracted from the Higgs searches at LEP, Tevatron and LHC. Another constraint, which must be accounted for, comes from the inclusive weak radiative B-meson Branching Ratio (BR) that proceeds through the quark-level transition of $b \to s\gamma$. A recent study [62], using results from the Belle Collaboration, places a 95% CL lower bound on the charged Higgs mass: $m_{H^\pm} > 580$ GeV. Therefore, we only select points above this mass value.

The algorithm specified above determines how a Markov chain evolves in the parameter space. Since each chain is independent, the different chains can be run in parallel, reducing the wall-clock time of the scan. The MCMC scan is performed over the 6-dimensional parameter space (m_H, $m_{H^\pm}$, m_A, $\cos(\beta-\alpha)$, $\tan\beta$, Z_7). The ranges and step-size of each parameter can be found in Tab. II. Other physical quantities are kept constant and their chosen values are listed in Tab. III. As the scan is computationally expensive, it is worth specifying what options were chosen for the scan: 400 independent chains were submitted, each for 20 hours on Dual 2.6 GHz Intel Xeon 8 core processor machines. With the given time limit, the setup yields an average chain length of O(10000) steps for each chain. Since the Markov chain first needs to find the minimum of the likelihood, then converge to thermal equilibrium, we account for this "warm-up" period, hence, the first 200 steps are discarded within every chain. The result of the MCMC scan is a data sample consisting of 4,259,823 points, before applying the theoretical constraints (perturbativity, unitarity, triviality and vacuum stability). A key feature of the MCMC scanning method is that the results can be interpreted in the Bayesian statistical framework, that is, the density of the points in the parameter space is proportional to the posterior probability of the model describing the data.

A post processing step is then performed where we calculate the production cross-sections and BRs of the (pseudo)scalars using `SusHi` [63] and `2HDMC` [64], respectively. This allows a direct link between experimental measurements and data interpretation within a given BSM theory, like (but not only) the 2HDM Type-II.

IV. BOUNDS ON THE 2HDM TYPE-II

In this section, we discuss the bounds that can be extracted on the six independent free parameters of the 2HDM Type-II simultaneously taking into account Higgs coupling strengths, EWPOs and the aforementioned theoretical constraints.

A. Experimental constraints

The values of the EWPOs, S, T and U within the 2HDM are derived in [65, 66] and implemented in `2HDMC`. The latter depends on the squared masses of the neutral Higgses through the F function [67], which commonly appears

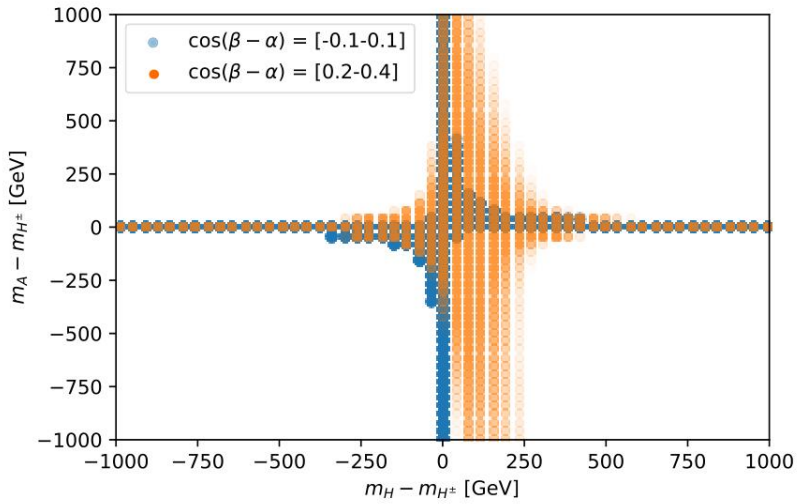

Figure 3: Allowed parameter points with $-0.04 \leq T \leq 0.24$ in the $(m_H - m_{H^\pm},\, m_A - m_{H^\pm})$ plane, for $|\cos(\beta-\alpha)| < 0.1$ and $0.2 < \cos(\beta-\alpha) < 0.4$.

in loop calculations:

$$F(x,y) = \frac{x+y}{2} - \frac{xy}{x-y}\ln\frac{x}{y}. \tag{10}$$

Here, $F(x,y)$ is a non-negative function, which is zero for $x = y$ and monotonically increasing with the difference between x and y. To simplify the notation, we use $F(A,B)$ denoting $F(m_A^2, m_B^2)$. The T parameter in the 2HDM can be expressed as:

$$\begin{aligned} T = c\Big\{ & \cos^2(\beta-\alpha)\Big[F(H^\pm,h) - F(A,h) - F(H^\pm,H) + F(H,A) \\ & + 3\left[F(Z,H) - F(W,H)\right] - 3\left[F(Z,h) - F(W,h)\right]\Big] \\ & + F(H^\pm,H) - F(H,A) + F(H^\pm,A)\Big\}, \end{aligned} \tag{11}$$

where c is

$$c = \frac{1}{\alpha_{\rm EM}}\frac{g^2}{64\pi^2 m_W^2}. \tag{12}$$

In the alignment limit, where $\cos(\beta-\alpha) \approx 0$, the T parameter simplifies to:

$$T = c\left[F(H^\pm,H) - F(H,A) + F(H^\pm,A)\right]. \tag{13}$$

From this we see that a mass degeneracy between A or H and $H^\pm$ induces a vanishing T parameter. Indeed, fixing either m_H or m_A to be equal to the charged Higgs mass is the rule-of-thumb generally taken in the literature to satisfy the EWPO constraints within the 2HDM. However, in the wrong-sign region where $\cos(\beta-\alpha) > 0$, by taking only the leading bound on the T parameter into account, this mass degeneracy can be relaxed to a large extent. This is shown Fig. 3, where we plot the allowed mass differences between the charged and neutral Higgs states compliant with the requirement $-0.04 \leq T \leq 0.24$. This choice is based on the GFitter analysis of Ref. [60], where $U = 0$ is imposed for extracting 95% CL bounds. As displayed by the orange points, for large $\cos(\alpha-\beta)$ values, that is in the wrong-sign domain, the m_H and m_A masses could simultaneously differ from the charged Higgs mass by roughly 250 GeV (or even more). Very large differences between scalar masses lead to large non-perturbative contributions,

though, therefore extreme cases are disfavoured (see later).

The net result, upon including in the MCMC scan the constraints coming from both the SM-like Higgs boson measurements and the EWPOs, is visualised in Fig. 4. There, we plot the allowed points in two parameter planes: $(\cos(\beta-\alpha), \tan\beta)$ (top-left) as well as $(m_H - m_{H^\pm}, m_A - m_{H^\pm})$ (top-right). In the first case, we also display the density of points while, in the second case, we split the point between the alignment and wrong-sign scenarios. The left plot in Fig. 4 is in fairly good agreement with the experimental fits displayed in Fig. 2, thus passing the goodness-of-fit test of the adopted `HiggsSignals` link. In the same figure, we also plot the two scenarios separately, the alignment one in the bottom-left and the wrong-sign one in the bottom-right frame. Furthermore, as it is interesting to measure the probability of a specific configuration of the parameter space being realised in Nature, we add colour gauges displaying the number of scan points being plotted.

B. Theoretical constraints

After discussing the limits on the 2HDM Type-II parameter space coming from direct and indirect experimental searches, in this section, we analyse the effect of theoretical constraints. The three major conditions can be concisely summarised as follows.

- Unitarity of the S matrix: the upper bound on the eigenvalues L_i of the scattering matrix of all Goldstone and Higgs 2-to-2 channels [68, 69] is fixed to be

$$|L_i| \leq 16\pi. \tag{14}$$

- Perturbativity: the quartic Higgs couplings should be small to justify the perturbative nature of the calculations

$$|\lambda_{H_i H_j H_k H_l}| \leq 8\pi. \tag{15}$$

- Stability of the potential: the quartic Higgs potential terms are bounded from below, in turn implying that [70]

$$\lambda_1 > 0, \quad \lambda_2 > 0, \quad \lambda_3 + \sqrt{\lambda_1 \lambda_2} > 0, \quad \lambda_3 + \lambda_4 - |\lambda_5| + \sqrt{\lambda_1 \lambda_2} > 0. \tag{16}$$

Out of these conditions, the stability and perturbativity of the potential pose the most severe constraints on the parameter space. In order to give an overview of the bounds coming from the theoretical constraints, in Fig. 5, we display the 2HDM Type-II parameter space regions excluded by the different constraints. For illustrative purposes, we have fixed the mass of the (pseudo)scalars to be $m_{H^\pm} = m_H = 600$ GeV and $m_A = 300$ and 400 GeV. The blue dots reflect the bounds arising from the requirement of unitarity. The effects are concentrated in the medium-high $\tan\beta$ range and for $|\cos(\beta-\alpha)| \geq 0.1$. Positive(negative) values of Z_7 disfavour negative(positive) values of $\cos(\beta-\alpha)$, shifting the excluded region on the right-(left-)hand side. The unitarity bounds do not affect the alignment and the wrong-sign domains, allowed by the `HiggsSignals` and EWPO constraints and represented by the blue(green and yellow) region at the 95%(90% and 68%) CL. The perturbativity constraint, represented by the magenta squares, extends the excluded region towards lower values of $\tan\beta$ and $|\cos(\beta-\alpha)|$ for the chosen value of the quartic Higgs coupling. The effect of Z_7 is the same as for unitarity. As displayed in the two upper plots of Fig. 5, for $Z_7 = 0$ the wrong-sign contour region is completely excluded by the perturbativity constraint (see left plot). By increasing the Z_7 value to $Z_7 = 0.6$, the parameter space opens up again (see right plot). According to this trend, even if not shown explicitly in the figure, one can deduce that negative Z_7 values tend to exclude the alignment region as well. Finally, the stability of the potential, represented by the black crosses, excludes all the negative values of $\cos(\beta-\alpha)$ and part of the positive values so to suppress almost completely the alignment domain. Summarising the effect of the three constraints coming from unitarity, perturbativity and stability, it is clear that negative values of Z_7 are disfavoured. For the chosen setup, no points lie in the alignment region; they are indeed concentrated in the wrong-sign domain (see lower right plot). More generally, by increasing the m_A value, the alignment and the wrong-sign scenarios get both populated again, the alignment contour at extremely low $\tan\beta$ values, in particular.

The conclusion to be drawn from this exercise is that the stability of the scalar potential enforces a lower bound on the pseudoscalar mass, m_A, in the alignment portion of the parameter space. We analyse this effect in more detail in the next section.

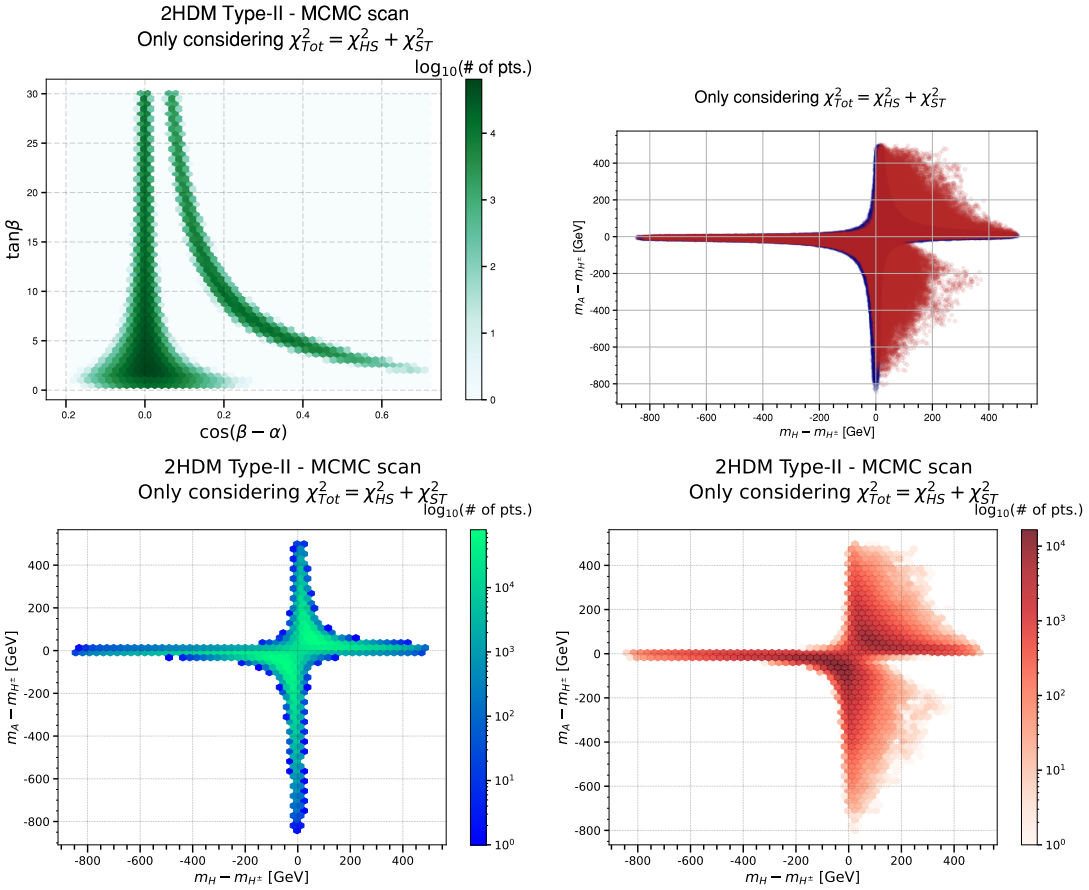

Figure 4: Distribution of the parameter space points on the $(\cos(\beta-\alpha), \tan\beta)$ (top-left) and $(m_H - m_{H^\pm}, m_A - m_{H^\pm})$ (top-right) planes from the MCMC scan in the 2HDM Type-II. In the mass plot, the alignment region is represented in blue while the wrong-sign one is superimposed in red, so that the latter obscure the former, hence we also show these separately: the blue-green points isolate the alignment limit scenario (bottom-left) while the red-orange ones isolate the wrong-sign configuration (bottom-right). The colour gauges measure the number of scan points plotted.

C. The role of m_A

In this subsection we investigate the conditions imposed by a stable scalar potential and their effect on the two limits of the model under consideration (2HDM Type-II): the alignment and wrong-sign domains. We use a collection of points from the MCMC scan, which passes the condition $\Delta\chi^2_{\rm tot} < (3\sigma$ CL upper limit) without imposing any other constraints. The stability inequalities in Eq. (16) are implemented step-by-step to be able to uniquely identify their effect on the parameter space. The following observations can be made.

- At the beginning (without imposing any of the stability conditions) there are points present in both the alignment and wrong-sign limit regions.
- The constraints $\lambda_1 > 0$ and $\lambda_2 > 0$ are targeting points from both regions irrespectively of the m_A value.
- There are surviving points in both regions after imposing $\lambda_1 > 0$ and $\lambda_2 > 0$.
- The condition $\lambda_3 + \sqrt{\lambda_1\lambda_2} > 0$ does not exclude any additional points for low m_A values but discards a large number of points exclusively from the alignment limit in the high m_A domain.
- The final constraint of $\lambda_3 + \sqrt{\lambda_1\lambda_2} + \lambda_4 - |\lambda_5] > 0$ again disfavours points from the alignment region independently on the m_A value. More importantly, this proves to exclude all of the points from the alignment limit region in

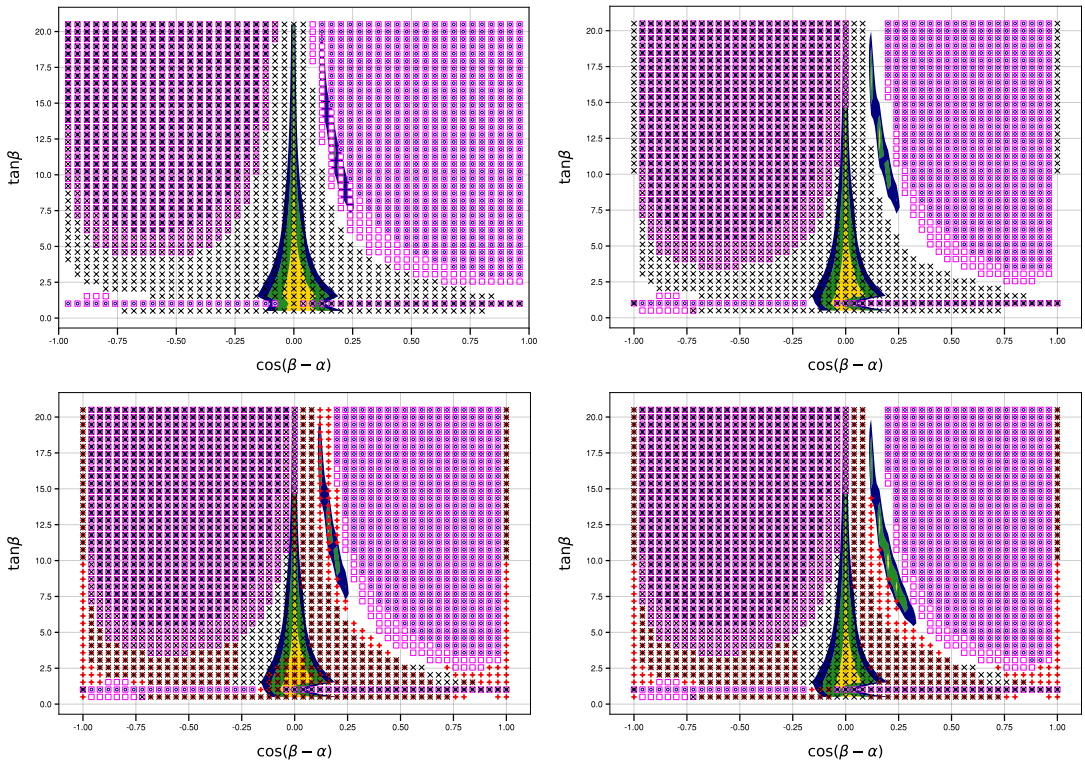

Figure 5: Distribution of the parameter space points on the $(\cos(\beta-\alpha), \tan\beta)$ plane excluded by the theoretical constraints of unitarity (blue hollow dots), perturbativity (magenta hollow squares) and stability (black crosses) in the 2HDM Type-II. The masses of the heavy Higgs, H and the charged Higgs $H^{\pm}$ are fixed at $m_{H^{\pm}} = m_H = 600$ GeV. The `HiggsSignals` and EWPO allowed regions correspond to the yellow, green, blue regions, with 1, 2 and 3σ CL compatibility respectively. Top row: in the left-hand plot, $m_A = 300$ GeV and $Z_7 = 0$; in the right-hand plot, $m_A = 300$ GeV and $Z_7 = 0.6$. Bottom row: in the left-hand plot, $m_A = 300$ GeV and $Z_7 = 0.6$; in the right-hand plot, $m_A = 400$ GeV and $Z_7 = 0.6$. The points excluded by `HiggsBounds` are also shown as red crosses.

the low-intermediate m_A range, with the exception of a handful of points at low $\tan\beta$. Contrary to this, the high m_A range contains surviving points in both regions after imposing all the conditions.

This result is visualised in the scatter plots of Fig. 6, where we display the (m_H, m_A) parameter space. The blue dots represent the alignment region while the red ones refer to the wrong-sign scenario. In these plots, we enforce the experimental bounds coming from `HiggsSignals` and EWPOs plus the theoretical constraints discussed above. We moreover set the lower bound on the charged Higgs mass at 600 GeV. In the left plot, one can see that very few points are left in the alignment region at low m_A. Those few are characterised by very small values of $\tan\beta$, as discussed previously. If we superimpose the `HiggsBounds` limits, even these remaining points disappear.

The global picture is shown in the right plot of Fig. 6. There one can see that, in the alignment limit of the 2HDM, the pseudoscalar state is required to be rather heavy: $m_A \geq 350$ GeV. Only in the wrong-sign scenario, it can in principle have a mass as light as $m_A \simeq 150$ GeV (see red dots), when Z_7 is rather large and positive, as shown in Fig. 5. This latter feature is the result of the effects coming from the perturbativity enforcement. This picture depends however on the limit that could be in future set on the charged Higgs mass. Raising the $m_{H^{\pm}}$ limit pushes the lower bound on m_A further up, in the alignment scenario. In the wrong-sign domain, one can still have light CP-odd Higgs masses at the price of stretching Z_7 towards large and positive values, $Z_7 \geq 1$, typically. This is in agreement with the findings given in Ref. [71]. Here, we have added a more detailed analysis of the effects coming from the individual constraints, highlighting in particular the role of the stability requirement on the scalar potential in setting a lower bound on the CP-odd Higgs mass in the alignment scenario.

In this section, we have described the framework and tools to extract the portion of the 2HDM Type-II parameter space that is allowed by present experimental constraints (summarised by EWPOs, `HiggsSignals` and `HiggsBounds`) and the theoretical requirements. We are now ready to discuss the possibilities that `Magellan`, the global scan tool we are presenting in this paper, offers to interpret the LHC data coming from a variety of up-to-date analyses within

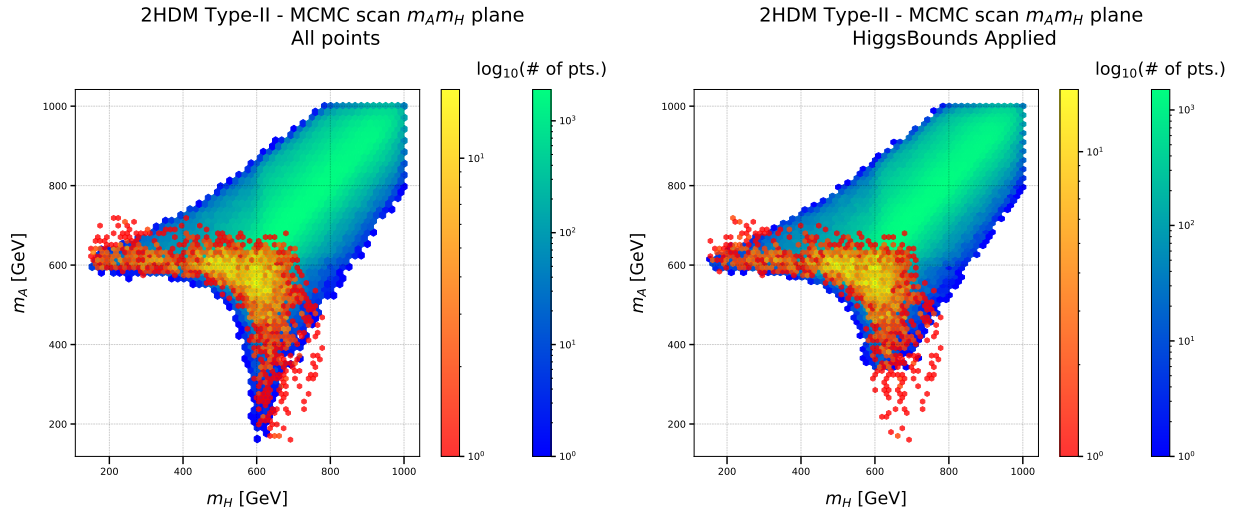

Figure 6: Distribution of the parameter space points on the (m_A, m_H) plane allowed by the theoretical constraints in the 2HDM Type-II. The bound on the charged Higgs mass is implemented as $m_{H^\pm} \geq 600$ GeV. In the left plot, the `HiggsSignals`, EWPOs and theoretical constraints are enforced. In the right plot, `HiggsBounds` limits are also added. The blue/green dots represent the alignment region while the red/yellow ones refer to the wrong-sign scenario. Two colour bars are shown next to each plot, both giving a logarithmic scale count to the colours used for the plot.

the specific model we are focussing on, the 2HDM Type-II.

V. DATA INTERPRETATION

In this chapter, we apply the methodology of the global scan tool, `Magellan`, to interpret the LHC data within the 2HDM Type-II. During the course of the MCMC scan, various experimental and theoretical properties linked to the individual parameter space points are computed and saved. This retained information allows to examine different aspects of the model from the same dataset. Any new unfolded experimental results can be then translated into direct bounds on the parameter space of the BSM scenario at hand, the 2HDM Type-II. The experimental results corresponding to a given observable, typically the 95% CL exclusion bound on the cross-section times BR, can be projected onto any two-dimensional sections of the full parameter space, thus allowing the extraction of limits on different parameters of the theory. The observables, i.e., cross-sections and BRs used for comparison, are computed by making use of `SusHi` and `2HDMC`.

As a working example, in the following, we consider the most recent ATLAS analysis of the process $pp \to A \to Zh \to Zb\bar{b}$ [72]. The search for the heavy CP-odd Higgs, A, decaying into a Z boson and the 125 GeV Higgs state, is performed by looking at final states with either two opposite-sign charge leptons (l^+l^- with $l = e, \mu$) or a neutrino pair ($\nu\bar{\nu}$) plus two b-jets at the 13 TeV LHC with a total integrated luminosity of $L = 36.1$ fb^{-1}. The 95% CL upper bound on the cross-section times BR as a function of the CP-odd Higgs mass m_A is shown in the left plot of Fig. 7. There, it is assumed that the possible signal comes from the pure gluon-gluon fusion production, while here we also account for quark-antiquark annihilation (which is generally subleading in comparison). In the right plot of the same figure, the theoretical cross-section times BR is computed within the 2HDM Type-II for the same m_A range. The different colours of the scatter points correspond to the values of $\cos(\alpha - \beta)$ shown in the top-right legend. The cross-section times BR depends on this parameter, sensibly. The couplings of the CP-odd Higgs, A, with the heavy quarks in the production subprocess and with the Z and h bosons in its subsequent decay all depend on $\cos(\alpha - \beta)$. Superimposed on this scatter-plot, there are the observed and expected curves taken from the ATLAS analysis (see left plot). From direct comparison, one can immediately see the excluded range of the CP-odd Higgs mass as a function of the $\cos(\alpha - \beta)$ value. This comparison can be further extended by taking into account the limit on the cross-section times BR expected in a near future with a luminosity $L = 300$ fb^{-1}. The projected exclusion bounds on $\cos(\alpha - \beta)$ show indeed a sensible improvement.

Beyond this, `Magellan` allows the extraction of a rich variety of information. The toolbox leverages the use of the

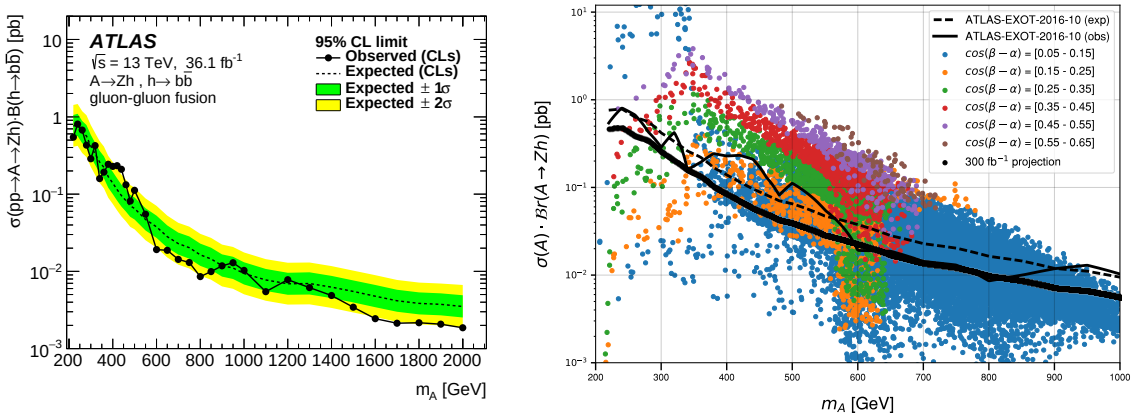

Figure 7: Left plot: 95% CL upper bound on the cross-section times BRs, $\sigma(pp \to A \to Zh \to Zb\bar{b})$, as a function of the CP-odd Higgs mass, extracted by ATLAS at the 13 TeV LHC [72]. Right-plot: Theoretical predictions for the same process $pp \to A \to Zh \to Zb\bar{b}$ within the 2HDM Type-II (here, $\sigma_A \equiv \sigma(pp \to A)$). The different colours of the points in the scatter plot represent different values of $\cos(\beta - \alpha)$. Superimposed, there is the ATLAS observed (expected) cross-section times BR given by the black solid (dashed) line. Finally, the heavy black curve shows the projection of the expect limit curve of the ATLAS analysis to a luminosity of $L = 300$ fb^{-1}.

`DataFrame` class of `pandas`, making a custom selection on the set of points relatively easy. Excluded (or allowed) points by a given theoretical constraint or experimental bound can then be projected onto any other plane, defined by the desired choice of model parameters or observables. In the specific case mentioned above, one can select points above the 95% CL upper bound on the observed cross-section times BR, given by the black solid line on the right plot of Fig. 7, and project those points in order to see the effect of that particular model-independent measurement on all the free parameters of the 2HDM Type-II. Note that, as the limits coming from the experimental analyses reported on HEPData (`https://www.hepdata.net/`) depend on the assumption made on the width of the new hypothetical Higgs bosons, when involved, the width of the (pseudo)scalar states is equally taken into account when extracting the bounds on the parameter space [73].

This feature is sketched in Fig. 8. Nine different 2D projections of model parameters and observables are shown, where first the points excluded by the aforementioned ATLAS analysis (red) are drawn and then non-excluded points (blue), irrespective of the other hidden parameters. One could also choose to visualise the results in the opposite order, that is, first the non-excluded points and then the excluded ones. In this way, the region of the parameter space tested by the specific experimental measurement at hand would stand out. The double option is implemented and shown on the `Magellan` interactive webpage [42].

From this subgroup of possible parameter spaces, one can already conclude that the low $\tan\beta$ region is the one being tested by the ATLAS analysis at the 13 TeV LHC [72], i.e., $\tan\beta \leq 5$ (c.f. the $(\cos(\beta-\alpha), \tan\beta)$ plane). There the range $\cos(\beta-\alpha) \geq 0.5$ is almost excluded for all m_A masses (c.f. the $(\cos(\beta-\alpha), m_A)$ projection). Thus, even if initially one built a colourless scatter plot of the $pp \to A \to Zh \to Zb\bar{b}$ rate as a function of m_A, with no information on the $\cos(\beta-\alpha)$ value of the individual points, the projection feature could shed light on the range of $\cos(\beta-\alpha)$ and $\tan\beta$ that one is testing. Of course, higher luminosities could be sensitive to larger values of $\tan\beta$ and smaller values of $\cos(\beta-\alpha)$, thus extending the search of new physics in particular in the wrong-sign region.

Also, by looking at the top-right plot showing the value of the width of the CP-odd Higgs over its mass as a function of $\cos(\beta-\alpha)$, one can see that the present analysis covers a parameter space up to where $\Gamma_A/M_A \leq 11\%$. But the possible values of this ratio extend up to $\Gamma_A/M_A \simeq 25\%$. This would imply that future experimental analyses should stop relying on the pure narrow width approximation and diversify their approach to include the search for wider resonances.

Projecting the points excluded by the expected limit on the production cross-section times BR of the process $pp \to A \to Zh$, at an integrated luminosity of $L = 300$ fb^{-1}, on the same projection planes as Fig. 8, one can see that a very significant portion of the parameter space will be under scrutiny. This is shown in Fig. 9 by the red scatter points. The region $\cos(\beta-\alpha) \geq 0.4$ can be excluded at such a luminosity, as shown by the top-right, middle-left and middle-central plots. Also the alignment region will start to disappear. This already gives a rather good idea of what will happen in the next data taking stages at the LHC.

This way of interpreting the model-independent experimental data within a given model is much more flexible and

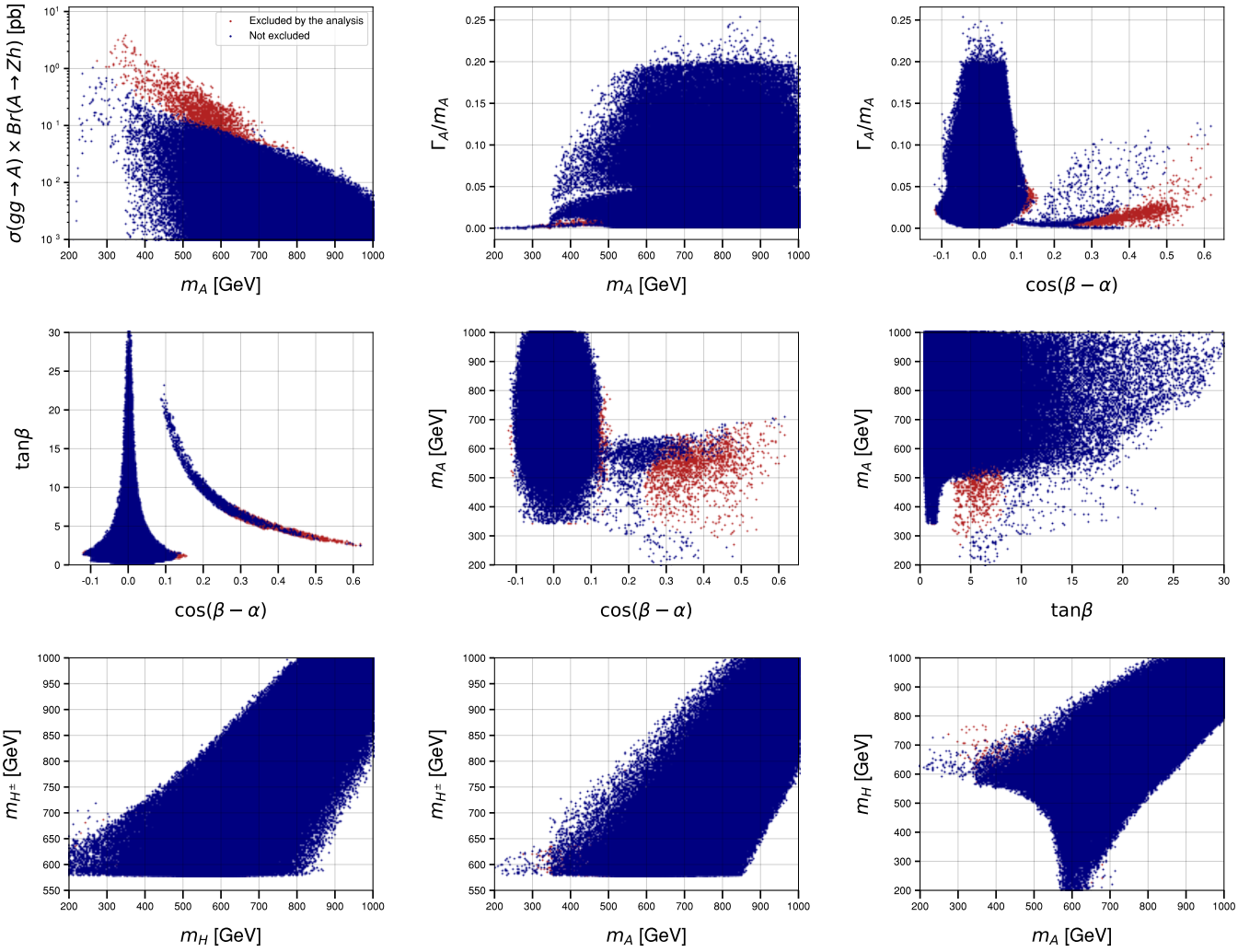

Figure 8: Projections of the 2HDM Type-II parameter and observables. The blue points are those allowed by `HiggsSignals`, EWPOs and theoretical constraints. The red ones are those excluded by the ATLAS analysis of the process $pp \to A \to Zh \to Zb\bar{b}$ with a luminosity of $L = 36.1$ fb^{-1}. (Recall that we are not enforcing `HiggsBounds` constraints here.) The white background corresponds to the region of parameter space failing against one or more of the limits from `HiggsSignals`, EWPOs and theoretical constraints.

complete than the the procedures adopted in the literature. Referring in particular to the most recent $pp \to A \to Zh$ search performed by ATLAS [72], one can notice that, for the interpretation of the cross-section times BR limits in the context of the 2HDM, the $H^{\pm}$, H and A bosons are assumed to be degenerate. In our analysis, the three masses can differ by 250 GeV and more, as detailed in Section IV A. Moreover, the visualisation of the limits at 95% CL on the 2HDM parameters as given in Ref. [72] is constrained and therefore partial. Bounds are in fact displayed on the $(\tan\beta, \cos(\beta-\alpha))$ plane, at a fixed value of the resonance mass m_A, and on the $(\tan\beta, m_A)$ plane, at a fixed value of $\cos(\alpha-\beta)$. The global scan presented in this paper can go beyond these limitations and display the full limits on any 2D plane, offering access to a rich variety of information.

A. 2HDM sensitivity of different measurements at the LHC

In this section, we analyse different possible measurements that can be performed at the LHC with the aim to show their sensitivity to a given set of model parameters within the 2HDM Type-II. We discuss first the relevance of the various channels, which might contain one or more Higgses as intermediate states, in covering portions of the

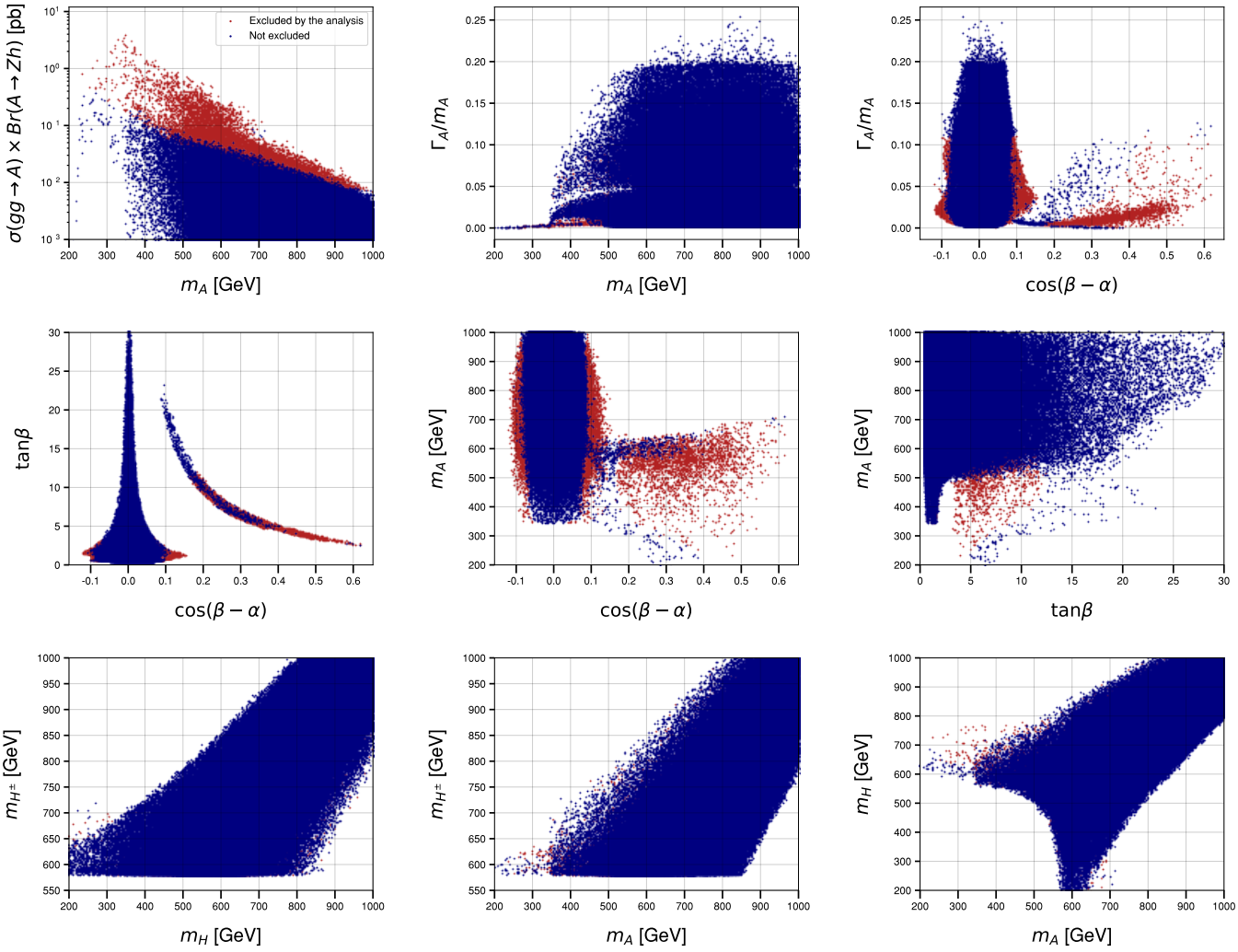

Figure 9: Projections of the 2HDM Type-II parameter and observables. The blue points are those allowed by `HiggsSignals`, EWPOs and theoretical constraints. The red ones are those excluded by the ATLAS analysis of the process $pp \to A \to Zh \to Zb\bar{b}$ projected to a luminosity of $L = 300$ fb^{-1}.

parameter space via the study of the BRs of the CP-odd A and the CP-even (heavy) H. Some of these portions show a partial overlap, some others are disjoint, as displayed in Fig. 10. There, by looking at the top row, one can clearly see that the $A \to t\bar{t}$ (red) and $A \to ZH$ (light blue) channels are quite complementary. The first one is sensitive to low $\tan\beta$ values (see top-left plot) and can cover a broad range of the mass spectrum where the A and H masses do not differ more than 200 GeV from each other and no hierarchy between them is made explicit (see top-right plot). On the contrary, the latter becomes relevant for low to medium $\tan\beta$ values and when an explicit hierarchy is in place. The A decay into down-type particles, b-quarks or τ-leptons, is enhanced at medium-to-high values of $\tan\beta$, as displayed by the green and yellow points in the top-left plot. Finally, the $A \to Zh$ mode is particularly sensitive to the large $\cos(\beta-\alpha)$ region and low to medium $\tan\beta$ values. If we instead look at the H decay modes (see bottom row), we see that they are dominated by the decays into $b\bar{b}$, $\tau^+\tau^-$ at high $\tan\beta$ and $t\bar{t}$, ZA at low $\tan\beta$. These decays are concentrated in the alignment region. This means that the processes mediated by the heavy H scalar are not sensitive to the region of large $\cos(\beta-\alpha)$. For probing or excluding this portion of the parameter space, that is, the wrong-sign scenario, one needs to rely on processes mediated by the A state, in particular, $A \to Zh$. Notice that in Fig. 10 some layering may occur if two or more criteria are satisfied, however, the overlapping regions are generally minimal so as to not change the visual picture given.

The decay modes give of course only a partial picture of the sensitivity of the experimental searches to the free parameters of the theory. One should consider the total rate, that is, production cross-section times BR(s), in order

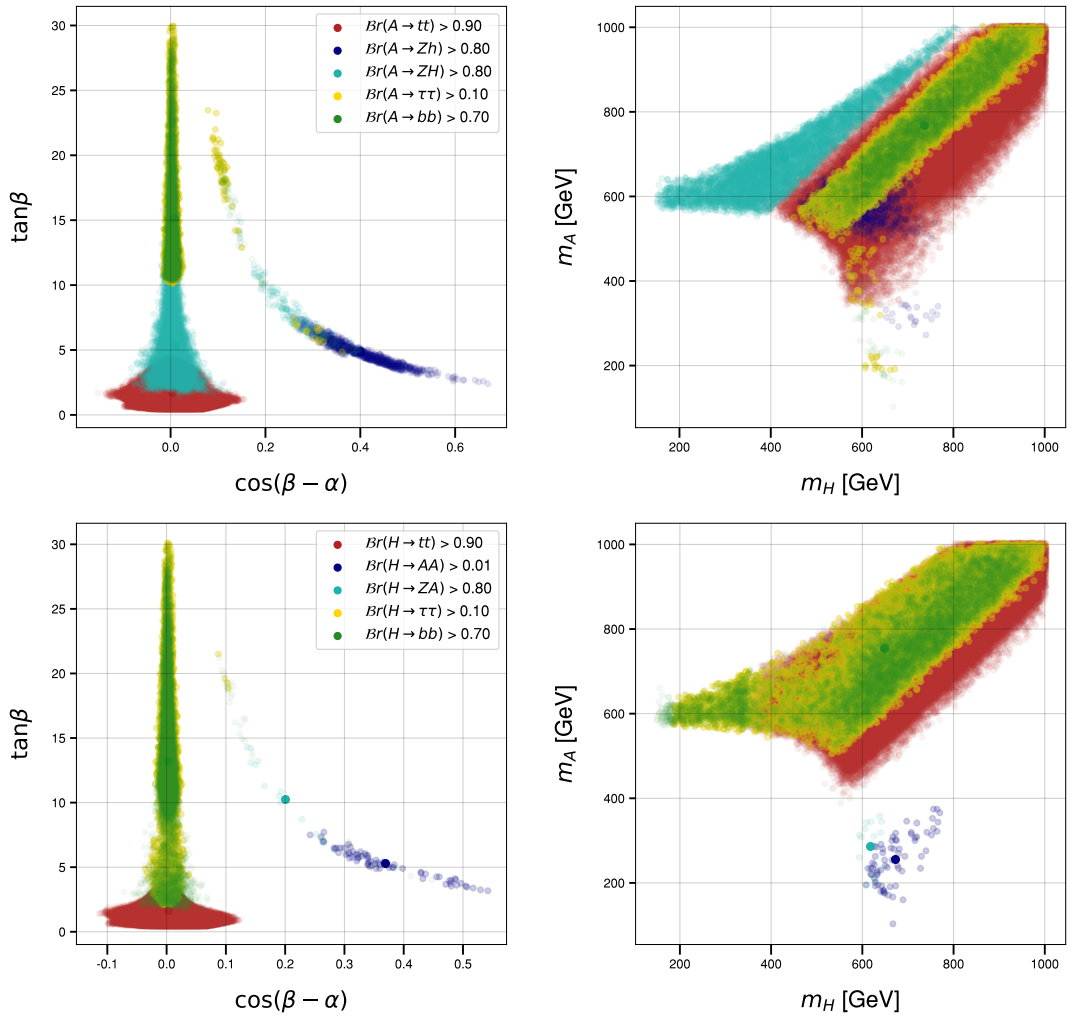

Figure 10: Top plots: regions of the two-dimensional parameter spaces with high BRs of the CP-odd Higgs, A, in the channels given in the legend of the top-left plot. Bottom plots: same for the heavy CP-even Higgs, H, decaying into the channels listed in the legend of the bottom-left plot.

to have a complete view. This is displayed in Fig. 11, where we plot the cross-section for the CP-odd Higgs in the bi-dimensional $(\cos(\beta-\alpha), \tan\beta)$ plane, and in Fig. 12, where we display the same observable for the heavy CP-even Higgs mediated processes. The magnitude of the total cross-section is given following the colour code on the right columns. For the A mediated processes, the cross-section can range from the order of 30 pb, corresponding to $pp \to A \to t\bar{t}$, to the order of a few fb, corresponding to the $\tau^+\tau^-$ channel. Analogous results hold for the H mediated processes.

VI. SUMMARY

In this paper, we have tensioned the 2HDM Type-II against data stemming from a variety of experimental contexts. We have included a wide range of results spanning from the old high precision LEP and SLC data, encoded into the so-called EWPOs, to the latest measurements performed at the LHC.

Compared to the existing literature, in this paper we have applied for the first time a new method that can improve the commonly used procedure for extracting bounds on the 2HDM parameter space. Our new numerical framework, called `Magellan`, and statistical techniques can be applied to any BSM scenarios. Here, we have taken as testing ground the 2HDM for two main reasons. Firstly, the 2HDM description of the scalar sector is representative of a large variety of BSM theories, where it is found to emerge in a natural way. Secondly, the 2HDM is characterised by a far

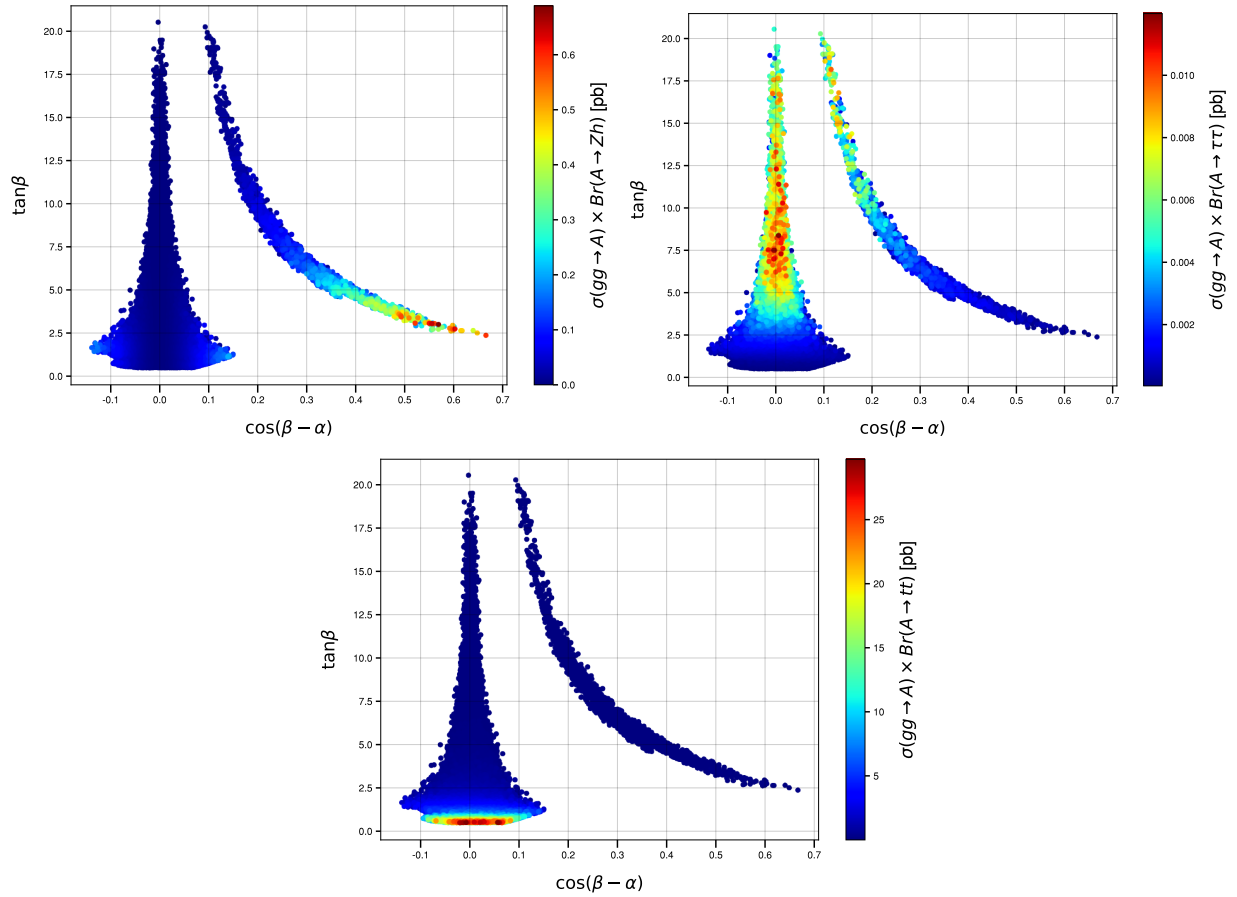

Figure 11: Magnitude of the total cross-section times BRs in the $(\cos(\alpha-\beta), \tan\beta)$ plane for four different processes mediated by the CP-odd Higgs, A. From top-left to bottom (clock-wise): $pp \to A \to Zh$, $pp \to A \to \tau^-\tau^+$ and $pp \to A \to t\bar{t}$.

from trivial multi-dimensional parameter space where the effectiveness of the new methods can be robustly proved.

`Magellan` is based on a Markov Chain Monte Carlo technique exploiting the Metropolis-Hastings algorithm (via `T3PS`), which features the following key elements: use of parallel processing when doing parameter scans, efficient data storage with fast I/O and interactive visualisation. This allows the user to explore any model in a complete and efficient way. The novelty of our approach is that the parameter space of any BSM theory can be projected onto any bi-dimensional plane while still retaining all underlying attributes of those points, hence, one always has the possibility of investigating the associations between the properties of its lower dimensional projections. The toolbox `Magellan` leverages the use of the `DataFrame` class of `pandas`, making a custom selection on the set of points relatively easy. The outcome is that excluded (or allowed) points by given theoretical constraints or experimental results corresponding to a given observable, typically the 95% CL exclusion bound on the cross-section times BR, can be therefore projected onto any 2D sections of the full parameter space, thus allowing the simultaneous extraction of limits on all the different parameters of the theory. A further scope of `Magellan` is that it can quickly predict the regions of the parameter space that can be accessible in a given search with the actual luminosity at hand, and show therein the characteristics of the new particles to be searched for (e.g., mass, width, BRs, etc.) thus allowing to improve the data analysis. This way of interpreting the model-independent experimental data within a given BSM theory is much more flexible and complete than the procedures adopted in the literature until now. `Magellan` is not published yet [41]. However, its website interactive dashboards can already be accessed via a public link. Through this website, the user can explore the full parameter space and exploit the phenomenological features of the model with ease.

In this paper, we have demonstrated some of its capabilities in relation to the mapping of the present and future LHC sensitivity to the dynamics of the aforementioned 2HDM, specifically, of Type-II. In this case, `Magellan` has been linked to external packages enabling one to test the 2HDM Type-II against experimental data, i.e., `HiggsBounds` and `HiggsSignals`, as well as to those enabling the prediction of the Higgs production and decay observables such as `SusHi` and `2HDMC`. This was done to assess whether the enlarged Higgs sector embedded in the 2HDM Type-II

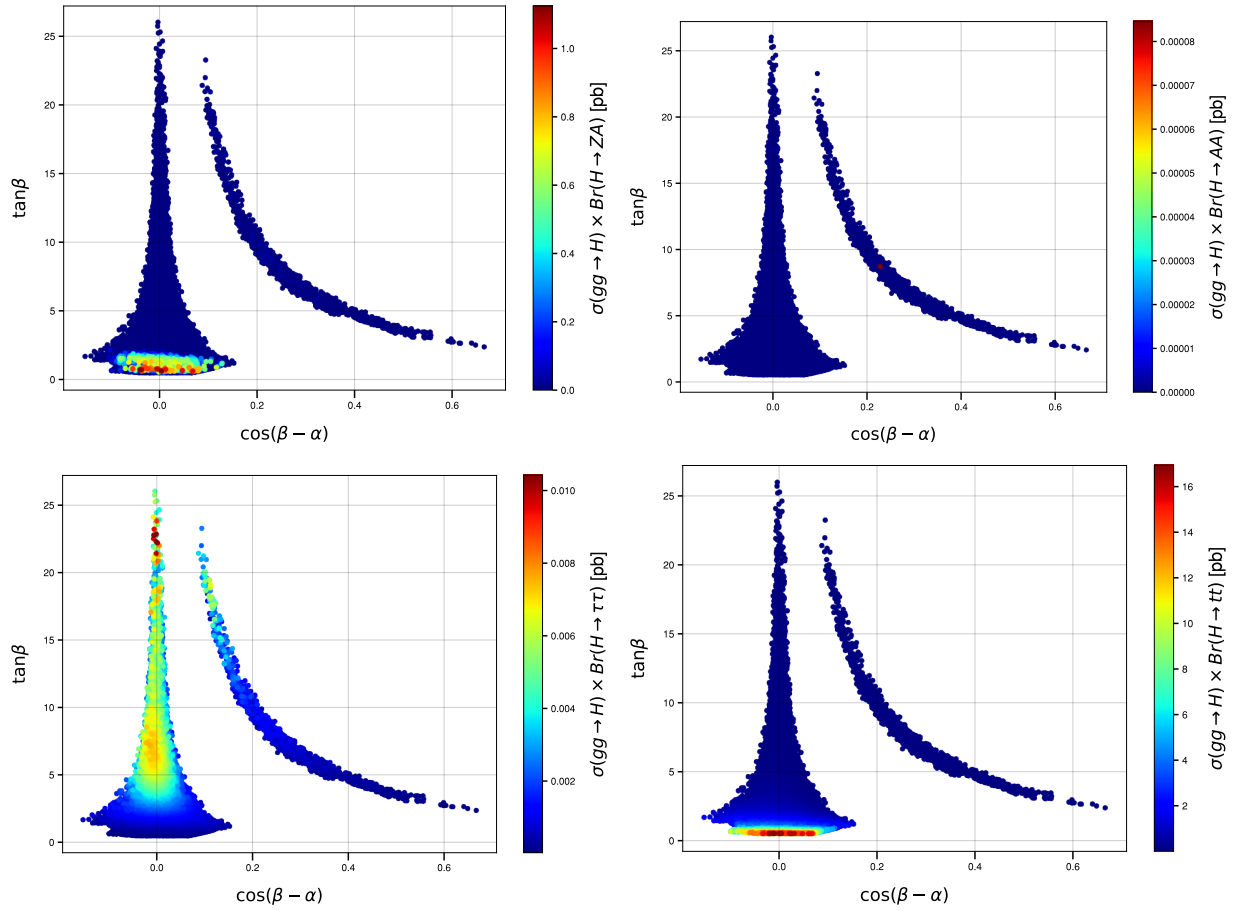

Figure 12: Magnitude of the total cross-section times BR in the $(\cos(\alpha-\beta), \tan\beta)$ plane for four different processes mediated by the heavy CP-even Higgs, H. From top-left to bottom-left (clock-wise): $pp \to H \to ZA$, $pp \to H \to AA$, $pp \to H \to t\bar{t}$ and $pp \to H \to \tau^-\tau^+$.

construct has survived experimental scrutiny to date and can thus be taken as a solid theoretical framework in which searches for new Higgs signals can be pursued at the LHC in the near future. In particular, we have shown that two distinct configurations of the parameter space of the 2HDM Type-II are currently compliant with all such data and also satisfy internal consistency requirements of the model, namely, the so-called wrong-sign' scenario (up to 1 TeV scale) and the alignment limit. Both of these can be probed during the upcoming runs of the LHC. The dynamics enabling one doing so are the production channels $pp \to A$ and $pp \to H$, i.e., those yielding, respectively, the heavy CP-even and CP-odd Higgs states belonging to the 2HDM Type-II spectrum. These extra Higgs bosons can in turn decay into a variety of modes, including chain decays of one Higgs boson into another, e.g., $A \to Zh$ and $H \to ZA$. These processes contain all the neutral Higgs bosons of such a BSM scenario (h represents the discovered SM-like Higgs state). The sensitivity of future LHC stages to all such production and decay modes was studied and it was argued that a combination of these could potentially pave the way to the detection of all such neutral states of the 2HDM Type-II. In particular, the discovery of a low or mid mass CP-odd Higgs boson, $m_A \leq 400$ GeV, could exclude the alignment limit of the 2HDM Type-II.

We have therefore equipped ourselves and readers with a new powerful and flexible framework, capable to test the hypothesis of an enlarged Higgs sector existing in Nature, as the `Magellan` voyage undertaken here can easily be repeated within any other BSM theory.

Acknowledgements

EA, DE and SM are supported in part through the NExT Institute. EA and SM also acknowledge support from the STFC Consolidated grant ST/L000296/1. All authors are grateful to Alex Owen at QMUL for having restored

the lost website and dashboard of the Magellan toolkit. They also acknowledge useful discussions with Shubhani Jain and Emmanuel Olaiya. The authors finally acknowledge the use of the IRIDIS High Performance Computing Facility and associated support services at the University of Southampton.

[1] G. Aad, *"Observation of a new particle in the search for the Standard Model Higgs boson with the ATLAS detector at the LHC,"* Physics Letters B **716**, 1 (2012), Observation of a new particle in the search for the Standard Model Higgs boson with the ATLAS detector at the LHC.

[2] S. Chatrchyan *et al.*, *"Observation of a new boson at a mass of 125 gev with the cms experiment at the lhc,"* Physics Letters B **716**, 30 (2012), Observation of a new boson at a mass of 125 GeV with the CMS experiment at the LHC.

[3] A. Celis, J. Fuentes-Martín, and H. Serôdio, *"Effective aligned 2HDM with a DFSZ-like invisible axion,"* Physics Letters B **737**, 185 (2014), effective aligned 2HDM with a DFSZ-like invisible axion.

[4] J. E. Kim, *"Light pseudoscalars, particle physics and cosmology,"* Physics Reports **150**, 1 (1987).

[5] J. Mrazek, A. Pomarol, R. Rattazzi, M. Redi, J. Serra, and A. Wulzer, *"The other natural two Higgs doublet model,"* Nuclear Physics B **853**, 1 (2011).

[6] E. Bertuzzo, T. S. Ray, H. de Sandes, and C. A. Savoy, *"On composite two Higgs doublet models,"* Journal of High Energy Physics **2013**, 1 (2013).

[7] K. Agashe, R. Contino, and A. Pomarol, *"The minimal composite Higgs model,"* Nuclear Physics B **719**, 165 (2005).

[8] S. D. Curtis, L. D. Rose, S. Moretti, and K. Yagyu, *"Supersymmetry versus Compositeness: 2HDMs tell the story,"* Physics Letters B **786**, 189 (2018).

[9] S. D. Curtis, L. D. Rose, S. Moretti, and K. Yagyu, *"A concrete composite 2-Higgs doublet model,"* Journal of High Energy Physics **2018** (2018), 10.1007/jhep12(2018)051.

[10] M. Aoki, S. Kanemura, and O. Seto, *"Neutrino Mass, Dark Matter, and Baryon Asymmetry via TeV-Scale Physics without Fine-Tuning,"* Phys. Rev. Lett. **102**, 051805 (2009).

[11] P. Ko, Y. Omura, and C. Yu, *"Dark matter and dark force in the type-I inert 2HDM with local $U(1)_H$ gauge symmetry,"* Journal of High Energy Physics **2014**, 1 (2014).

[12] J. Cao, P. Wan, L. Wu, and J. M. Yang, *"Lepton-specific two-Higgs-doublet model: Experimental constraints and implication on Higgs phenomenology,"* Phys. Rev. D **80**, 071701 (2009).

[13] A. Broggio, E. J. Chun, M. Passera, K. M. Patel, and S. K. Vempati, *"Limiting two-higgs-doublet models,"* Journal of High Energy Physics **2014**, 58 (2014).

[14] L. Wang and X.-F. Han, *"A light pseudoscalar of 2hdm confronted with muon g-2 and experimental constraints,"* Journal of High Energy Physics **2015**, 39 (2015).

[15] *"The Higgs Hunter's Guide,"* Front. Phys. **80**, 1 (1990), the Higgs Hunter's Guide.

[16] A. Djouadi, *"The anatomy of electroweak symmetry breaking Tome II: The Higgs bosons in the Minimal Supersymmetric Model,"* Physics Reports **459**, 1 (2008), the anatomy of electroweak symmetry breaking Tome II: The Higgs bosons in the Minimal Supersymmetric Model.

[17] G. Branco, P. Ferreira, L. Lavoura, M. Rebelo, M. Sher, and J. P. Silva, *"Theory and phenomenology of two-Higgs-doublet models,"* Physics Reports **516**, 1 (2012), theory and phenomenology of two-Higgs-doublet models.

[18] M. Baak, M. Goebel, J. Haller, A. Hoecker, D. Kennedy, K. Mönig, M. Schott, and J. Stelzer, *"Updated status of the global electroweak fit and constraints on new physics,"* The European Physical Journal C **72** (2012), 10.1140/epjc/s10052-012-2003-4.

[19] R. Lafaye, T. Plehn, and D. Zerwas, *"SFITTER: SUSY parameter analysis at LHC and LC,"* (2004), arXiv:hep-ph/0404282 .

[20] R. R. d. Austri, R. Trotta, and L. Roszkowski, *"A markov chain monte carlo analysis of the cmssm,"* Journal of High Energy Physics **2006**, 002–002 (2006).

[21] C. Strege, G. Bertone, D. Cerdeño, M. Fornasa, R. R. d. Austri, and R. Trotta, *"Updated global fits of the cmssm including the latest lhc susy and higgs searches and xenon100 data,"* Journal of Cosmology and Astroparticle Physics **2012**, 030–030 (2012).

[22] C. Strege, G. Bertone, F. Feroz, M. Fornasa, R. R. d. Austri, and R. Trotta, *"Global fits of the cmssm and nuhm including the lhc higgs discovery and new xenon100 constraints,"* Journal of Cosmology and Astroparticle Physics **2013**, 013–013 (2013).

[23] P. Bechtle, K. Desch, and P. Wienemann, *"Fittino, a program for determining mssm parameters from collider observables using an iterative method,"* Computer Physics Communications **174**, 47–70 (2006).

[24] P. Bechtle, K. Desch, M. Uhlenbrock, and P. Wienemann, *"Constraining susy models with fittino using measurements before, with and beyond the lhc,"* The European Physical Journal C **66**, 215–259 (2010).

[25] P. Bechtle, T. Bringmann, K. Desch, H. Dreiner, M. Hamer, C. Hensel, M. Krämer, N. Nguyen, W. Porod, X. Prudent, and et al., *"Constrained supersymmetry after two years of lhc data: a global view with fittino,"* Journal of High Energy Physics **2012** (2012), 10.1007/jhep06(2012)098.

[26] S. Kraml, T. Quang Loc, D. T. Nhung, and L. D. Ninh, *"Constraining new physics from higgs measurements with lilith: update to lhc run 2 results,"* SciPost Physics **7** (2019), 10.21468/scipostphys.7.4.052.

[27] J. Bernon and B. Dumont, *"Lilith: a tool for constraining new physics from higgs measurements,"* The European Physical

Journal C **75** (2015), 10.1140/epjc/s10052-015-3645-9.
[28] O. Buchmueller, R. Cavanaugh, A. De Roeck, J. R. Ellis, H. Flaecher, S. Heinemeyer, G. Isidori, K. A. Olive, F. J. Ronga, and G. Weiglein, *"Likelihood functions for supersymmetric observables in frequentist analyses of the cmssm and nuhm1,"* The European Physical Journal C **64**, 391–415 (2009).
[29] O. Buchmueller, R. Cavanaugh, D. Colling, A. De Roeck, M. J. Dolan, J. R. Ellis, H. Flächer, S. Heinemeyer, G. Isidori, K. Olive, and et al., *"Implications of initial lhc searches for supersymmetry,"* The European Physical Journal C **71** (2011), 10.1140/epjc/s10052-011-1634-1.
[30] O. Buchmueller, R. Cavanaugh, A. De Roeck, M. J. Dolan, J. R. Ellis, H. Flächer, S. Heinemeyer, G. Isidori, D. Martínez Santos, K. A. Olive, and et al., *"Supersymmetry in light of 1/fb of lhc data,"* The European Physical Journal C **72** (2012), 10.1140/epjc/s10052-012-1878-4.
[31] O. Buchmueller, R. Cavanaugh, A. De Roeck, M. J. Dolan, J. R. Ellis, H. Flächer, S. Heinemeyer, G. Isidori, J. Marrouche, D. Martínez Santos, and et al., *"Higgs and supersymmetry,"* The European Physical Journal C **72** (2012), 10.1140/epjc/s10052-012-2020-3.
[32] O. Buchmueller, R. Cavanaugh, A. D. Roeck, M. J. Dolan, J. R. Ellis, H. Flächer, S. Heinemeyer, G. Isidori, J. Marrouche, D. M. Santos, and et al., *"The cmssm and nuhm1 after lhc run 1,"* The European Physical Journal C **74** (2014), 10.1140/epjc/s10052-014-2922-3.
[33] P. Athron, C. Balazs, T. Bringmann, A. Buckley, M. Chrząszcz, J. Conrad, J. M. Cornell, L. A. Dal, H. Dickinson, and et al., *"Gambit: the global and modular beyond-the-standard-model inference tool,"* The European Physical Journal C **77** (2017), 10.1140/epjc/s10052-017-5321-8.
[34] P. Athron, C. Balázs, T. Bringmann, A. Buckley, M. Chrząszcz, J. Conrad, J. M. Cornell, L. A. Dal, J. Edsjö, and et al., *"A global fit of the mssm with gambit,"* The European Physical Journal C **77** (2017), 10.1140/epjc/s10052-017-5196-8.
[35] F. Rajec, W. Su, M. White, and A. G. Williams, *"Exploring the 2hdm with global fits in gambit,"* EPJ Web of Conferences **245**, 06022 (2020).
[36] V. Maurer, *"T3PS: tool for parallel processing in parameter scans,"* (2015), arXiv:1503.01073 .
[37] Wes McKinney, *"Data Structures for Statistical Computing in Python," Proceedings of the 9th Python in Science Conference*, , 51 (2010).
[38] J. D. Hunter, *"Matplotlib: A 2d graphics environment,"* Computing In Science & Engineering **9**, 90 (2007).
[39] Bokeh Development Team, *Bokeh: Python library for interactive visualization* (2014).
[40] J.-L. R. Stevens, P. Rudiger, and J. A. Bednar, in *Proceedings of the 14th Python in Science Conference*, edited by K. Huff and J. Bergstra (2015) pp. 59–66.
[41] C. Byers, D. Englert, S. Jain, S. Moretti, and E. Olaiya, (in).
[42] The Magellan Collaboration, "Interactive dashboards," `https://pprc.qmul.ac.uk/projects/magellan/2HDM/`.
[43] G. Aad, B. Abbott, D. Abbott, A. Abed Abud, K. Abeling, D. Abhayasinghe, S. Abidi, O. AbouZeid, N. Abraham, H. Abramowicz, and et al., *"Combination of searches for higgs boson pairs in pp collisions at s=13tev with the atlas detector,"* Physics Letters B **800**, 135103 (2020).
[44] E. Accomando, M. Chapman, A. Maury, and S. Moretti, *"Below-threshold CP-odd Higgs boson search via $A \to Z^* h$ at the LHC,"* Phys. Lett. B **818**, 136342 (2021), arXiv:2002.07038 [hep-ph] .
[45] S. Davidson and H. E. Haber, *"Basis-independent methods for the two-higgs-doublet model,"* Phys. Rev. D **72**, 035004 (2005).
[46] S. L. Glashow and S. Weinberg, *"Natural conservation laws for neutral currents,"* Phys. Rev. D **15**, 1958 (1977).
[47] E. A. Paschos, *"Diagonal neutral currents,"* Phys. Rev. D **15**, 1966 (1977).
[48] H. E. Haber and O. Stal, *"New LHC benchmarks for the CP-conserving two-Higgs-doublet model,"* European Physical Journal C **75**, 1 (2015), arXiv:1507.04281 .
[49] P. M. Ferreira, R. Santos, J. F. Gunion, and H. E. Haber, *"Probing wrong-sign Yukawa couplings at the LHC and a future linear collider,"* Physical Review D - Particles, Fields, Gravitation and Cosmology **89** (2014), 10.1103/PhysRevD.89.115003, arXiv:1403.4736 .
[50] G. Aad, *"Combined measurements of higgs boson production and decay using up to 80 fb^{-1} of proton-proton collision data at $\sqrt{s}$ = 13 tev collected with the atlas experiment,"* Phys. Rev. D **101**, 012002 (2020).
[51] A. M. Sirunyan *et al.*, *"Combined measurements of Higgs boson couplings in proton–proton collisions at $\sqrt{s} = 13$ TeV,"* Eur. Phys. J. C **79**, 421 (2019), arXiv:1809.10733 [hep-ex] .
[52] P. Basler, P. M. Ferreira, M. Mühlleitner, and R. Santos, *"High scale impact in alignment and decoupling in two-Higgs doublet models,"* Phys. Rev. **D97**, 095024 (2018), arXiv:1710.10410 [hep-ph] .
[53] P. M. Ferreira, S. Liebler, and J. Wittbrodt, *"$pp \to A \to Zh$ and the wrong-sign limit of the two-Higgs-doublet model,"* Phys. Rev. **D97**, 055008 (2018), arXiv:1711.00024 [hep-ph] .
[54] N. Metropolis, A. W. Rosenbluth, M. N. Rosenbluth, A. H. Teller, and E. Teller, *"Equation of state calculations by fast computing machines,"* The Journal of Chemical Physics **21**, 1087 (1953), http://dx.doi.org/10.1063/1.1699114 .
[55] W. K. Hastings, *"Monte carlo sampling methods using markov chains and their applications,"* Biometrika **57**, 97 (1970).
[56] P. Bechtle, S. Heinemeyer, O. Stål, T. Stefaniak, and G. Weiglein, *"HiggsSignals: Confronting arbitrary Higgs sectors with measurements at the Tevatron and the LHC,"* Eur. Phys. J. **C74**, 2711 (2014), arXiv:1305.1933 [hep-ph] .
[57] P. Bechtle, S. Heinemeyer, T. Klingl, T. Stefaniak, G. Weiglein, and J. Wittbrodt, *"Higgssignals-2: probing new physics with precision higgs measurements in the lhc 13 tev era,"* The European Physical Journal C **81** (2021), 10.1140/epjc/s10052-021-08942-y.
[58] G. Aad and al., *"Combined measurement of the higgs boson mass in pp collisions at $\sqrt{s} = 7$ and 8 tev with the atlas and cms experiments,"* Phys. Rev. Lett. **114**, 191803 (2015).

[59] G. Aad, B. Abbott, J. Abdallah, O. Abdinov, B. Abeloos, R. Aben, O. S. AbouZeid, N. L. Abraham, H. Abramowicz, and et al., *"Measurements of the higgs boson production and decay rates and constraints on its couplings from a combined atlas and cms analysis of the lhc pp collision data at $\sqrt{s}$=7 and 8 tev,"* Journal of High Energy Physics **2016** (2016), 10.1007/jhep08(2016)045.

[60] M. Baak, J. Cúth, J. Haller, A. Hoecker, R. Kogler, K. Mönig, M. Schott, and J. Stelzer, *"The global electroweak fit at nnlo and prospects for the lhc and ilc,"* The European Physical Journal C **74**, 3046 (2014).

[61] P. Bechtle, O. Brein, S. Heinemeyer, O. Stål, T. Stefaniak, G. Weiglein, and K. E. Williams, *"*HiggsBounds – 4*: Improved Tests of Extended Higgs Sectors against Exclusion Bounds from LEP, the Tevatron and the LHC,"* Eur. Phys. J. **C74**, 2693 (2014), arXiv:1311.0055 [hep-ph] .

[62] M. Misiak and M. Steinhauser, *"Weak radiative decays of the b meson and bounds on $m_{H^\pm}$ in the two-higgs-doublet model,"* The European Physical Journal C **77**, 201 (2017).

[63] R. V. Harlander, S. Liebler, and H. Mantler, *"SusHi: A program for the calculation of Higgs production in gluon fusion and bottom-quark annihilation in the Standard Model and the MSSM,"* Comput. Phys. Commun. **184**, 1605 (2013), arXiv:1212.3249 [hep-ph] .

[64] D. Eriksson, J. Rathsman, and O. Stal, *"2HDMC: Two-Higgs-Doublet Model Calculator Physics and Manual,"* Comput. Phys. Commun. **181**, 189 (2010), arXiv:0902.0851 [hep-ph] .

[65] W. Grimus, L. Lavoura, O. Ogreid, and P. Osland, *"The Oblique parameters in multi-Higgs-doublet models,"* Nucl. Phys. B **801**, 81 (2008), arXiv:0802.4353 [hep-ph] .

[66] W. Grimus, L. Lavoura, O. Ogreid, and P. Osland, *"A Precision constraint on multi-Higgs-doublet models,"* J. Phys. G **35**, 075001 (2008), arXiv:0711.4022 [hep-ph] .

[67] M. Veltman, *"Limit on mass differences in the weinberg model,"* Nuclear Physics B **123**, 89 (1977).

[68] I. F. Ginzburg and I. P. Ivanov, *"Tree-level unitarity constraints in the most general two Higgs doublet model,"* Physical Review D - Particles, Fields, Gravitation and Cosmology **72**, 1 (2005), arXiv:0508020 [hep-ph] .

[69] S. Kanemura, T. Kubota, and E. Takasugi, *"Lee-Quigg-Thacker bounds for Higgs boson masses in a two-doublet model,"* Physics Letters B **313**, 155 (1993), arXiv:9303263 [hep-ph] .

[70] N. G. Deshpande and E. Ma, *"Pattern of symmetry breaking with two Higgs doublets,"* Phys. Rev. D **18**, 2574 (1978).

[71] J. Bernon, J. F. Gunion, H. E. Haber, Y. Jiang, and S. Kraml, *"Scrutinizing the alignment limit in two-Higgs-doublet models. II. m_H=125 GeV,"* Phys. Rev. D **93**, 035027 (2016), arXiv:1511.03682 [hep-ph] .

[72] ATLAS Collaboration, *"Search for heavy resonances decaying into a W or Z boson and a Higgs boson in final states with leptons and b-jets in 36 fb^{-1} of $\sqrt{s} = 13$ TeV pp collisions with the ATLAS detector,"* JHEP **03**, 174 (2018), [Erratum: JHEP11,051(2018)].

[73] Experimental limits are available up to $\Gamma_A/m_A < 11\%$.